ABRASIVE WATERJET PROCESS PARAMETERS OPTIMIZATION

A thesis presented to the faculty of the Graduate School of Western Carolina University in partial fulfillment of the requirements for the degree of Master of Science in Engineering Technology

By
Frederick Malm

Advisor: Dr. Basel Alsayyed
Assistant Professor
School of Engineering + Technology

Committee Members:

Prof. Wes Stone, School of Engineering + Technology
Dr. Chaitanya Borra, School of Engineering + Technology

MAY 2024

ACKNOWLEDGMENTS

I am deeply grateful to express my sincere appreciation to my thesis advisor, Dr. Basel Alsayyed, for his invaluable mentorship, unwavering support, and constant encouragement throughout this research. His experience, patience, and dedication have been instrumental in shaping this study. I will remember your willingness to equip me with all the necessary professional skills to prepare me for the industry.

I want to thank Dr Wes Stone and Dr. Chaitanya Borra for their insightful feedback and constructive criticism, which have directed and enriched the quality of this work. Also, I want to thank Dr. Paul Yanik for his guidance and for ensuring I am on track and spending quality time on the research.

Finally, to my family, whose unwavering support has been my foundation throughout my educational journey at Western Carolina University, and to my fellow graduate students for sharing their experiences and motivation have inspired me, I express my deepest appreciation.

TABLE OF CONTENTS

Contents

ABSTRACT vii
CHAPTER 1: INTRODUCTION 1
CHAPTER 2: LITERATURE REVIEW 3
2.1 Abrasive Waterjet Machining Process 3
2.2 Fundamental principles of abrasive waterjet cutting 4
2.3 Overview of Key Process Parameters 4
2.4 Previous Research on AWJM Process Parameters 6
2.5 Factors influencing surface roughness in machining processes. 7
2.5.1 Effect of Pressure on Surface Roughness 8
2.5.2 Effect of Abrasive flowrate on Surface roughness 9
2.5.3 Effect of Transverse speed on Surface roughness 10
2.5.4 Effect of standoff distance on Surface roughness 11
2.5.5 Effect of Material Thickness on Surface Roughness 13
2.5.6 Influence of process input factors on Kerf angle and Material removal rate 15
2.6 Optimization Techniques and Approaches 15
2.6.1 Taguchi Optimization 15
2.6.2 Taguchi Grey Relational Analysis Optimization 17
CHAPTER 3: METHODOLOGY 19
3.1 Material Selection 19
3.2 Machine (WARD Jet -A-0612) 20
3.2.1 System Software 20
3.3 Identification of Key Process Parameters 22
3.3.1 Selection of Factor Levels 22
3.3.2 Determination of Response Variables 23
3.4 Experimental Design 25
3.4.1 Specimen Design 27
3.5 Experimental Setup 28
3.5.1 Measured Result for the Output Responses 29
3.6 Taguchi Design of Experiment 30
3.6.1 Taguchi Single Response Optimization 30
3.6.2 Analysis of Variance (ANOVA) 32

3.7 Multi-Response Optimization 32
3.7.1 Taguchi – Grey Relational Analysis 32
3.7.2 Taguchi-Grey Relational Analysis Model 33
CHAPTER 4: RESULTS 36
4.1 Single Response Optimization- Taguchi 36
4.2 Optimization Analysis for Aluminum 6061-T6 36
4.2.1 Surface Roughness (Ra) 36
4.2.2 Kerf Angle 39
4.2.3 Material Removal Rate (MRR) 42
4.2.4 Evaluation of Experimental Data 44
4.3 Optimization analysis for 1020 Carbon Steel 45
4.3.1 Surface Roughness (Ra) 45
4.3.2 Kerf Angle 47
4.3.3 Material Removal Rate (MRR) 50
4.3.4 Evaluation of Experimental Data 52
4.4 Summary of the Single Response Optimization for Both Metals 53
4.5 Taguchi- Grey Relational Analysis Optimization- Multi Response 53
4.5.1 Aluminum 6061-T6 54
4.5.2 1020 Carbon steel 56
4.6 Summary for Both Optimization Methods 58
CHAPTER 5: DISCUSSION 60
5.1 Single Response Optimization 60
5.2 Influence of material thickness on the output response 60
5.2.1 Surface Roughness (Ra) 60
5.2.1 Kerf Angle 61
5.2.2 Material Removal Rate (MRR) 62
5.3 Multiple Response Optimization 63
5.4 Confirmation Test 65
CHAPTER 6: Conclusion and Future Works 66
6.1 Conclusion of Study 66
6.2 Key Conclusions from the Study 66
REFERENCES 69

LIST OF FIGURES

Figure 1. Schematic of the AWJ Cutting Head (Radovanović, 2020)..... 5
Figure 2. Schematic impacts of standoff distance on Workpiece (μMachining) 12
Figure 3. Deviation in Jet Cutting Intensity through Different Layers of Thickness(Khan & Gupta, 2020) 14
Figure 4. WARDJet A-0612 20
Figure 5. WARDCAM Interface - WARDDJet..... 21
Figure 6. MOVE Interface - WARDJet..... 21
Figure 7. Representation of the kerf Geometry(Fuse et al., 2021)..... 24
Figure 8. SPI Tester II Surface Roughness 25
Figure 9. Specimen Dimension..... 28
Figure 10. Setup for the Experimental Runs..... 28
Figure 11. Flow chart for the Taguchi Grey Relational Optimization (Qazi et al., 2020) 33
Figure 12. Main Effect Plot for the S/N Ratios – Surface Roughness (Ra)..... 37
Figure 13. Actual vs. Predicted data for 5 and 3 Factors Respectively 39
Figure 14. Main Effect Plot for the S/N Ratios – Kerf Angle..... 40
Figure 15. Actual vs. Predicted data for 5 and 1 Factor Respectively..... 41
Figure 16. Main Effect Plot for S/N Ratios - MRR 43
Figure 17. *Actual vs. Predicted data for 5 and 2 Factors Respectively*..... 44
Figure 18. Probability Plot for the Three Output Responses – Aluminum 6061 – T6..... 44
Figure 19. Main Effect for S/N Ratios – Surface Roughness (Ra) 46
Figure 20. Actual vs. Predicted data for 5 and 1 Factors Respectively 47
Figure 21. Main Effect Plot for S/N Ratios – Kerf Angle..... 48
Figure 22. Actual vs. Predicted data for 5 and 3 Factors Respectively..... 49
Figure 23. Main Effect Plot for S/N Ratios - MRR 51
Figure 24. Actual vs. Predicted data for 5 and 3 Factors Respectively..... 52
Figure 25. *Probability Plot for the Three Output Responses – 1020 Carbon Steel*..... 52
Figure 26. Main Effect Plot for the GRA Optimization..... 57

LIST OF TABLES

Table 1. WARDJet Machine Specification 20
Table 2. Input Factors and Their Levels for Aluminum 6061 T6 23
Table 3. Input Factors and Their Levels for 1020 Carbon Steel 23
Table 4. Taguchi OA for 1020 Carbon Steel 26
Table 5. Taguchi OA for Aluminum 6061-T6 27
Table 6. Measured Responses for Aluminum 6061-T6 29
Table 7. Measured Responses for 1020 Carbon Steel 30
Table 8. Response Table for S/N Ratios – Surface Roughness (Ra) 37
Table 9. Analysis of Variance for Surface Roughness (Ra) 38
Table 10. Response Table for S/N Ratios – Kerf Angle 39
Table 11. Analysis of Variance for Kerf Angle 41
Table 12. Response Table for S/N Ratios - MRR 42
Table 13. Analysis of Variance for MRR 43
Table 14. Response Table for S/N Ratios – Surface Roughness (Ra) 45
Table 15. Analysis of Variance for Surface Roughness (Ra) 46
Table 17. Response Table for S/N Ratios – Kerf Angle 47
Table 18. Analysis of Variance for Kerf Angle 49
Table 20. Response Table for S/N Ratios - MRR 50
Table 21. Analysis of Variance for MRR 51
Table 22. Results from the Optimal Settings for Each Response- Single Response Optimization 53
Table 23. Response Table for S/N Ratios - GRG 54
Table 24. Analysis of Variance for GRA - Aluminum 6061-T6 56
Table 25. Response Table for S/N Ratios - GRA 56
Table 26. Analysis of Variance for GRA- 1020 Carbon Steel. 58
Table 27. Summary of Single Response and Multi Response Optimization (Taguchi-Grey Relational Analysis) 59

NOMENCLATURE

DOE	Design of Experiment
GRA	Grey Relational Analysis
MRR	Material Removal Rate
ANOVA	Analysis of Variance
AWJM	Abrasive Waterjet Machining
KA	Kerf Angle
JP	Jet Pressure
CFRP	Carbon Fiber Reinforced Plastic
AWJ	Abrasive Waterjet
CAD	Computer-Aided Design
MPa	Megapascal
OA	Orthogonal Array
S/N	Signal to Noise
SiB	Smaller-is-Better
LiB	Larger-is-Better
GRG	Grey Relational Grade
GRC	Grey Relational Coefficient
Ra	Arithmetic Average Roughness
MRO	Multi Response Optimization

ABSTRACT

ABRASIVE WATERJET PROCESS PARAMETERS OPTIMIZATION

Abrasive waterjet machining has gained significant importance in the manufacturing sector for its efficiency and versatility in cutting various materials without generating heat, making it suitable for temperature-sensitive materials. It presents a significant challenge in achieving high-quality surface finishes, especially with varying metal thicknesses. The study aimed to use the Taguchi Design of Experiment (DOE) coupled with Grey Relational Analysis (GRA) to optimize the single and multi-responses for Aluminum 6061-T6 and 1020 carbon steel. The experiments were conducted using the A-0612 WARD Jet machine, and data analysis was performed using Minitab and Microsoft Excel. The Taguchi orthogonal array was used to design the experimental runs(L27). This experimental research explored the effects of influential input factors such as water pressure, abrasive mass flow rate, traverse speed, standoff distance, and material thickness, where each input factor was tested at three levels. The GRA methodology was used to optimize the output responses, such as surface roughness (Ra), Kerf angle, and material removal rate (MRR), simultaneously to achieve high surface quality, and the results were compared to those of the single response optimization. The study highlights the significant impact of material thickness on the variation in machined metal surface quality. The main effect plots and analysis of variance (ANOVA) reveal that aluminum thicknesses of 1.016 and 4.825mm and carbon steel thicknesses of 6.35 and 9.525 mm consistently result in the desirable output response. These high-quality results were achieved using optimal settings derived from the findings of the optimization model.

Keywords: Grey Relational Analysis (GRA), Non-traditional machining, Optimization, Taguchi DOE, Waterjet, Analysis of Variance (ANOVA)

CHAPTER 1: INTRODUCTION

Abrasive Waterjet Machining (AWJM) has emerged as a cutting-edge method for precision cutting across diverse industries, including aerospace, automotive, and mining (*Chandravadhana et al., 2021*). It offers distinct advantages over traditional cutting techniques by employing highly pressurized water mixed with abrasive particles (garnet) to cut various materials efficiently (*Ozcan et al., 2021*). However, despite its widespread adoption, AWJM encounters a significant challenge in achieving high-quality surface finishes, mainly when there are variations in machining metal thickness. In applications where joint integrity and stress concentration reduction are critical for component performance, optimizing AWJM parameters becomes paramount to ensure the desired surface finish quality.

The general research problem centers on achieving high-quality surface finishes in Abrasive Waterjet Machining, especially when presented with varying metal thicknesses. Within this problem, the specific research question arises: How does material thickness affect the output responses in AWJM, and what are the optimal settings to simultaneously achieve the highest quality response? This research has three primary objectives:

1. To conduct experiments to assess the impact of material thickness on output responses.
2. To analyze the main effects and interactions of input factors on each response, mainly focusing on Surface Roughness (Ra), Material Removal Rate (MRR), and Kerf angle (α)
3. To optimize input factors concurrently to achieve the highest quality response.

Abrasive Water Jet Machining (AWJM) is a well-established, non-traditional method in machining processes. Its distinction lies in the absence of tool contact, which effectively reduces the Heat-Affected Zone, making it ideal for temperature-sensitive materials (*Spadło et al., 2021*). Using a high-velocity stream of water combined with abrasive material, AWJM can effectively remove material from various workpieces. However, the effectiveness of AWJM heavily relies on the control of multiple factors inherent in the process. Optimizing these process parameters is crucial for enhancing AWJM's output responses. The AWJM process consists of diverse machining parameters where each input factor is essential in determining the final output quality (*Çetin, 2021*). Previous research has primarily focused on optimizing these input factors to achieve desired outcomes. Material thickness emerges as a significant factor influencing the quality of the cut. Therefore, fine-tuning the machining parameters becomes imperative for achieving precision in AWJM. Recognizing the complex relationship among these input factors is key as it directly impacts the overall efficacy of the Abrasive Waterjet Machining (AWJM) process (*Llanto et al., 2021b*). Given the process input factors' nonlinear impact on the output response, precise optimization of process parameters in AWJM becomes imperative for consistently achieving desired outcomes (Manoj et al., 2018).

CHAPTER 2: LITERATURE REVIEW

This chapter provides an in-depth review of the existing literature on Abrasive Waterjet Machining (AWJM) process parameters optimization, with a specific focus on material thickness alongside other influential input parameters influence on surface roughness (Ra), kerf angle and material removal rate (MRR). The review covers the various optimization methodologies, including Taguchi design of experiment and Grey Relational Analysis (GRA), and their applications in improving machining quality. The following literature highlights the current gaps and limitations in the existing literature, which this study aims to address through the proposed study.

2.1 Abrasive Waterjet Machining Process

Abrasive waterjet cutting (AWJM) is a flexible and widely used process for cutting and shaping materials, including metals, ceramics, and composites(*Vigneshwaran et al., 2018*). It has been found efficient in machining hard metals. In contrast, traditional cutting methods often prove challenging due to the inherent challenges posed by their high tensile strength and resistance to deformation(*A. Arun et al., 2023*). Among non-traditional machining techniques, the water jet machine stands out for its vast potential in manufacturing applications. It is exceptionally well suited for machine materials that are challenging to handle with conventional techniques because of its capacity to generate minimum heat-affected zones(Gangadharan et al., 2022a). This characteristic is essential, especially when dealing with materials sensitive to thermal alterations.

The AWJ process is widely used in many industrial production sectors because it offers a comprehensive solution to companies looking for accurate and effective cutting procedures with less thermal impact. According to Jiao et al. (2023), integrating specialized process technologies,

particularly waterjet cutting and other non-traditional machining methods, is essential in machining carbon fiber-reinforced composites. Many industries use these materials extensively, including automotive, aerospace, and military applications.

2.2 Fundamental principles of abrasive waterjet cutting.

During the abrasive waterjet (AWJ) machining, a high-pressure water jet is directed through a smaller nozzle and mixed with abrasive grit particles. This high-velocity jet is aimed at a specific material zone to erode and remove the desired material *(A. Arun et al., 2023).* The impact of the abrasive particles on the workpiece surface causes material erosion *(Shastri et al., 2021)*. The main components of an abrasive waterjet cutting system include a high-pressure pump, an abrasive hooper, a nozzle, and a cutting head. The cutting parameters, such as abrasive size, pressure, and other process parameters, can be adjusted to achieve the desired surface finish and cutting speed (*Gangadharan et al., 2022a*). However, these parameters must be optimized for different metal thicknesses to achieve the best results. Several control parameters influence the performance of AWJM, and optimizing these parameters has been researched and applied to find the optimal combinations for the process *(Chakraborty & Mitra, 2018).*

2.3 Overview of Key Process Parameters

Gangadharan et al. categorizes the process parameters that affect the output response of abrasive water jet-cutting processes. These parameters are categorized into four types: hydraulic, mixing and acceleration, cutting, and abrasive. The hydraulic parameters involve controlling water pressure, water orifice diameter, and water flow rate. The mixing and acceleration parameters involve the focus diameter and focus length. The cutting parameters include traverse speed, number of passes, standoff distance, and impact angle. Finally, the abrasive parameters involve the control of abrasive mass flow rate, particle diameter, particle size distribution,

particle shape, and particle (*Kuttan et al., 2021*). The study provides valuable insights into the interplay between these variables and cutting performance.

The AWJM cutting process depends on the parameters that affect the machining output response, such as the Kerf angle, surface roughness, and material removal rate. Most of the process input parameters are correlated with each other, where the change in one factor can influence the desired output. Therefore, it is necessary to determine the relations among the various process input parameters and how they affect the objective function depending on the required output response (*Çetin, 2021*). The AWJM process utilizes pressurized water through a cutting head equipped with an orifice, mixing chamber, and nozzle. Abrasive particles are introduced, creating an abrasive mixture directed toward the workpiece for material removal*(Radovanović, 2020*). As shown in Figure 1, various process parameters can be controlled to achieve the desired output response.

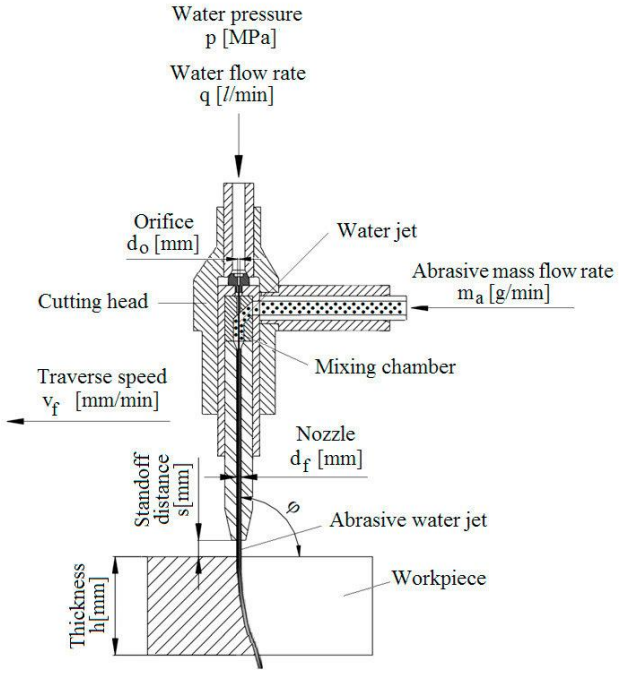

Figure 1. *Schematic of the AWJ Cutting Head (Radovanović, 2020)*

2.4 Previous Research on AWJM Process Parameters

Most study findings revealed that the variation of process parameters strongly influences the performance of AWJ machining. However, the extent of this influence depends on the magnitude of the parameter changes and the material's machinability (*Hascalik et al., 2007*). *Singh and Vishvakarma (2015)* state that various process factors impact the surface finish characteristics produced by touching base on jet pressure and standoff distance of the nozzle from the target: abrasive flow rate, Traverse rate, and work materials. During the cutting operation, the process parameters are critical in determining the outcome (*Shukla & Singh, 2017*). According to *Shukla and Singh*, achieving the desired quality in the AWJM process requires careful attention to the optimum setting of process parameters.

Few researchers have explored the impact of these parameters on the performance of the process; their findings suggest that even small changes can significantly affect the output response (*Pal et al., 2017a*). Process parameters are crucial for achieving optimal results in Abrasive water jet machining (AWJM). The most commonly used parameters in AWJM experiments, as most researchers employ, include water pressure, traverse speed, abrasive flow rate, and standoff distance (*Pon Selvan et al., 2018*). In a study conducted by *Pon Selvan et al*., these parameters' effects on cut depth were examined, and the findings concluded that high water pressure is preferred to achieve optimal cutting performance. However, in a study conducted by *Tiwari et al.*, the effects of water pressure, abrasive flow rate, and traverse speed on the machining of Alumina ceramic (Al2O3) with a thickness of 18mm and a length, width, and height of 96mm, 55mm, and 38mm, respectively, were investigated. The results revealed that all the input parameters, including pressure, traverse speed, and abrasive flow rate, significantly affected the output responses, such as material removal rate (MRR), surface roughness (SR), and kerf angle.

Gangadharan et al.(2022b) highlight the significance of carefully selecting and optimizing specific process parameters and their corresponding levels to achieve desired outcomes in various manufacturing processes. The slight adjustments to these parameters can have an observable impact on the resulting output response, highlighting the importance of precise control and optimization to ensure consistent and high-quality results (*S. Alsoufi, 2017*). In optimizing process parameters and improving manufacturing efficiency in abrasive waterjet machining, it is essential to understand the relationship between input factors and finishing quality.

2.5 Factors influencing surface roughness in machining processes.

Surface roughness (Ra) is a measure of the finish of the machined component, indicating the degree of smoothness or roughness on the surface (*Shastri et al., 2021*). Surface roughness is the top priority in machining, with a priority level of 73.38%. This highlights the importance of achieving high-quality surface finishes in the machining process. Material removal rate (MRR) is also crucial, and the researchers dedicated significant effort to optimizing surface roughness (*Chakraborty et al., 2019*). Surface roughness quantifies the smoothness or irregularity of a machined surface. In abrasive waterjet machining (AWJM), achieving smooth surfaces is paramount for meeting quality standards and functional requirements across various industries (*Saravanan et al., 2020*).

Saravanan et al. identified surface roughness as one of the output responses determined by the performance of AWJM. However, other process input factors, including process parameters, material properties, nozzle characteristics, and ambient conditions, affect surface roughness in AWJM. This study focuses on the effects of these process parameters: water pressure, abrasive flow rate, federate, standoff distance, and material thickness on surface

roughness, kerf angle, and material removal rate and provides optimal settings for optimizing the machining process. By examining the relationships between input parameters and surface finish quality, this study investigates AWJM technology and facilitates the development of more efficient and reliable machining processes.

2.5.1 Effect of Pressure on Surface Roughness

Kumaran et al. (2017) investigated the surface roughness in abrasive waterjet machining of carbon fiber-reinforced plastics (CFRP) and found that increasing the jet pressure (JP) led to a smoother finish. Specifically, higher JP values resulted in better separation of the carbon fibers from the matrix, creating a more uniform top and bottom kerf width. Increasing water pressure can improve the surface finish of the material by allowing the cutting jet to remove more material. Increasing jet pressure reduces surface roughness due to the smooth erosion on the surface or through the workpiece material, which smooths out the surface and results in a more even finish *(Ravi Kumar et al., 2018*). However, there is a limit to how much pressure is beneficial, and too much pressure can cause problems.

Finding the optimal pressure level is essential to balance the surface finish and these potential drawbacks. The finish of the material will be rougher and more uneven if the force applied by the cutting jet is higher. Higher forces can cause the material to be cut more aggressively, resulting in a rougher finish (*Khalid et al., 2019*). *Manivannan et al. (2019)* highlight in their study that the pressure of the cutting process is a significant factor that plays a significant role in affecting the kerf angle of the machined surface. Water pressure is a substantial process parameter in abrasive waterjet (AWJ) machining.

Increasing water jet pressure correlates with greater penetration depth into the material and higher material removal rates. It also affects the distribution of water and abrasive particles

within the jet stream (*Tiwari et al., 2018*). The water pressure directly determines the energy possessed by the jet. With increased water pressure, the cut depth and the surface become smoother (*Saravanan et al., 2020*). Cetin (2021) implies that high pressure can improve surface quality. However, it is essential to acknowledge that even slight variations in feed rate and abrasive flow can significantly affect the process, highlighting the sensitivity of these parameters.

2.5.2 Effect of Abrasive flowrate on Surface roughness

According to the study by Tiwari et al. (2018), the workpiece's surface roughness decreases as the abrasive flow rate increases. The increased abrasive flow rate leads to more significant impacts from abrasive particles on the workpiece surface, potentially resulting in a smoother surface. In other words, more abrasive particles are striking the surface at higher speeds, reducing SR. While increasing the abrasive flow rate can lead to a smoother workpiece surface, it can also decrease cutting efficiency due to increased interactions between the abrasive particles and the material being cut (*Chakraborty & Mitra, 2018*). The mass rate of abrasive particles and other factors can significantly impact a process's machining efficiency and surface quality. It is crucial to control this parameter to achieve optimal results carefully (*Xiaochu et al., 2019*).

In abrasive water jet (AWJ) machining, two primary material removal modes occur due to micro-cutting: cutting and deformation/plowing. The deformation/plowing mode involves the abrasive particles deforming and pushing the workpiece material aside, while the cutting mode involves the particles cutting into the material. Both mechanisms contribute to the material removal process in AWJ machining. Natural abrasives like garnet and synthetic abrasives, like silicon carbide and aluminum oxide, are employed in the AWJ machining process (*Natarajan et*

al., 2020). Natarajan et al. conducted an in-depth review of the significance of an optimum supply of abrasives in AWJ machining processes. They found that the right amount and type of abrasives can significantly improve cutting performance and surface finish. As the flow rate increases, more abrasive particles strike the material, increasing wear and tear and reducing the machined part's smoothness.

As the abrasive flow rate exceeds a certain threshold, the process can become saturated, leading to challenges in effectively transferring momentum to the abrasive particles. Reduced surface roughness suggests that the abrasive particles may no longer effectively remove material. In other words, there may be an optimal flow rate for the process, beyond which further increases in flow rate do not result in improved surface finish (Saravanan et al., 2020). When the abrasive flow rate was at its highest, the surface roughness was observed to be lower. The relationship between the feed rate and surface roughness indicates that higher feed rates result in smoother surfaces (*Çetin, 2021*).

2.5.3 Effect of Transverse speed on Surface roughness

Traverse speed was the most influential factor affecting surface roughness, while standoff distance was the least significant factor (*Pal et al., 2017b*). The speed of the cutting nozzle across the workpiece surface significantly impacts the roughness of the surface. In other words, faster traverse speeds produce rougher surfaces, while slower traverse speeds produce smoother surfaces. Sharma et al. (2018) found that jet transverse speed significantly impacts surface roughness, accounting for approximately 54.53% of the total variation. In contrast, stand-off distance had a relatively minor influence on surface roughness. Ravi et al. (2018) found that surface roughness was highly influenced by Transverse speed and Standoff distance on Tungsten Carbide.

Kusnurkar and Singh (2019) optimized AWJM input parameters using three abrasive garnets (Brown Fused Alumina, White Aluminum Oxide) on MS2062 and compared their performance. They found that traverse speed significantly affects surface finish. *Edriys et al. (2020)* conducted a study to investigate the effect of process parameters on some responses using the Taguchi method optimization at the end of the study. They found that the surface roughness of the workpiece increased with an increase in traverse speed and other process parameters such as feed rate and depth of cut. The traverse speed significantly impacts the workpiece's surface finish, indicating that optimizing this parameter can improve surface quality. The findings from the study indicated that the traverse speed is the most influential parameter for achieving improved output responses.

The primary determinant affecting the surface roughness of the workpiece was identified as the traverse speed of the nozzle or jet travel speed, with jet pressure ranking as the subsequent influential factor (*Khan & Gupta, 2020*). The findings from the study by *Joel and Jeyapoovan (2021)* indicate that the traverse speed is the most influential parameter for achieving improved output responses. When the traverse speed surpasses the ideal threshold, the water abrasive particles cannot sufficiently cut the material, resulting in unsatisfactory erosion outcomes. The interconnectedness of AWJM process variables emphasizes how they collectively influence surface roughness Ra, illustrating their interrelated nature (*Shastri et al., 2021*).

2.5.4 Effect of standoff distance on Surface roughness

The distance (standoff) between the nozzle and the workpiece affects the depth of the cut *(Viswanath et al., 2018*). *Ahmed et al. (2018)* found that standoff distance is not a significant factor in surface quality but becomes substantial when interacting with other control factors. As the standoff distance increases, it leads to a rougher surface finish, while reducing this distance

results in a smoother finish (*Bui, 2020*). Increasing the standoff distance enlarges the opening, generating a more comprehensive jet stream with a broader coverage area. Conversely, reducing the standoff distance forms a narrower opening, resulting in a more focused, concentrated jet stream with a smaller coverage area. When the standoff distance is longer, the water jet has more room to extend before initiating the cutting process.

The ideal standoff distance for optimal results is 2 mm (*Çetin, 2021*). Figure 2 shows the effects of different height differences on the standoff of machined parts. At high standoff distances, the jet becomes divergent, resulting in a low density of abrasive particles and an expansion of the jet. This expansion decreases material removal from the machining zone, resulting in a rough surface. Therefore, it is desirable to maintain a low standoff distance to ensure the kinetic energy of the jet is maintained, resulting in smoother surfaces (*Fuse et al., 2021*)

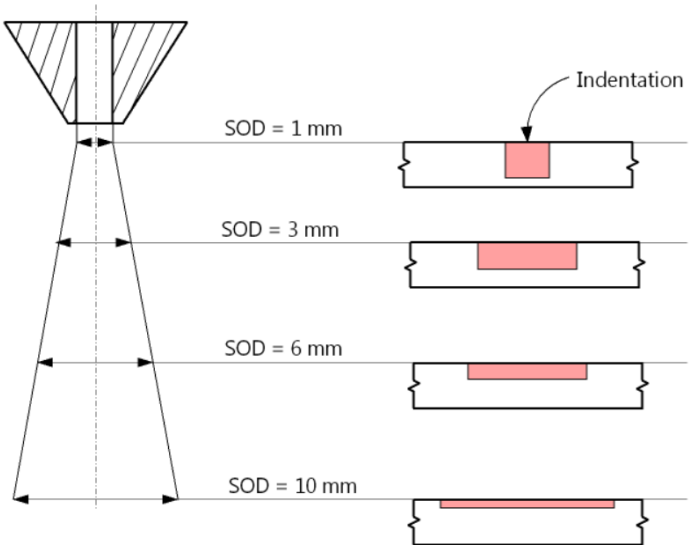

Figure 2. *Schematic impacts of standoff distance on Workpiece (µMachining)*

Adjusting the standoff distance reduces abrasive particles' velocity, decreasing the pressure of impinged water on the workpiece. As the cutting tool moves along the workpiece,

there is a gradual decrease in the depth of the cut, resulting in a tapered cut. Therefore, optimizing the standoff distance is paramount for achieving the desired cut quality (*Shastri et al., 2021*).

2.5.5 Effect of Material Thickness on Surface Roughness

Most existing research on abrasive water jet machining (AWJM) primarily focuses on optimizing parameters such as water pressure, abrasive flow rate, traverse speed, and standoff distance to minimize surface roughness. Numerous studies have demonstrated the significant impact of these parameters on surface roughness, highlighting their importance in achieving desired machining outcomes. However, despite the extensive investigation into these parameters, more exploration of the influence of material thickness on surface roughness in AWJM needs to be conducted. The machined material's thickness directly influences the machined part's surface roughness.

The thickness of the material affects the jet energy and the amount of material being removed. When the material thickness increases, the jet energy is dissipated over a larger area, decreasing jet impact and erosion rate. As a result, the material removal rate decreases while surface roughness increases. On the other hand, when the material thickness decreases, the jet energy is concentrated over a smaller area, resulting in a higher jet impact and erosion rate, leading to an increase in material removal rate and a decrease in surface roughness. According to a study *by Khan and Gupta (2020)*, the roughness of machined surfaces can be a significant challenge when working with thick sections.

The intensity of the jet penetration, which travels from one level to another, decreases as the thickness of the workpiece increases, leading to a rougher finish and reduced surface quality. Such alterations could potentially have implications for the overall performance of the

component. In their study, Adam and Khan incrementally examined the surface roughness of machined surfaces regarding the bulk thickness. They found that the surface roughness increased as the thickness of the workpiece increased due to the decreased intensity of the jet penetration, therefore highlighting the importance of considering the thickness of the workpiece when machining thick sections to maintain a smooth finish and optimal surface quality. Figure 3 illustrates the lag observed at various thickness sections as the water jet travels through the material.

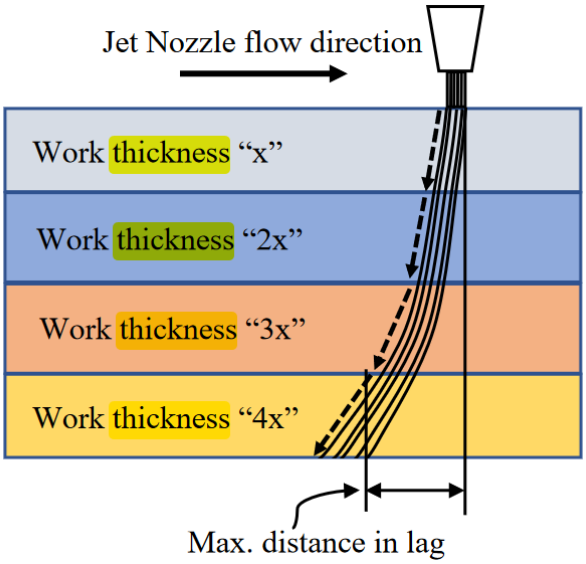

Figure 3. *Deviation in Jet Cutting Intensity through Different Layers of Thickness(Khan & Gupta, 2020)*

Adam and Khan's study found that as the material's thickness increases, the surface finish's quality decreases, resulting in less desirable finishes for thicker materials than thinner ones. *Edriys et al. (2020)* discovered that as the thickness of the material increases, the surface roughness also increases. This rise in surface roughness is due to the larger area of the cut surface and the presence of more layers and flaws in thicker materials. As a result, the difference

between the peaks and valleys of the surface becomes more pronounced, leading to a poor finish with significant waviness.

2.5.6 Influence of process input factors on Kerf angle and Material removal rate

In addition to surface roughness, the kerf angle is another relevant output response that affects the quality of the cut. The deviation between the top and bottom cuts is caused by the loss of kinetic energy as the pressurized water jet travels through the metal at a high standoff distance, leading to a kerf angle (*Llanto et al., 2021a*). According to *Llanto et al*., reducing the traverse speed can lower the kerf angle while increasing the traverse speed maximizes the material removal rate.

The MRR is directly proportional to the machining speed, so higher MRR values correspond to faster machining rates, which serves as a performance metric that provides valuable insight into the efficiency of the process (*Karkalos et al., 2024*). *Dekster et al. (2023)* study found that high water pressure with considerable traverse speed maximizes the MRR and reduces the kerf angle, which is confirmed by another study by *Karmiris-Obratański et al. (2021)*, which indicates that increasing traverse speed leads to a low MRR.

2.6 Optimization Techniques and Approaches

2.6.1 Taguchi Optimization

The optimization of machine parameters is an essential aspect of manufacturing processes, as it can significantly affect the quality, productivity, and cost-effectiveness of the production process. In recent years, various optimization techniques have been widely used in machining processes to improve their performance. The study aims to provide an overview of machining processes' most commonly used optimization techniques, including Taguchi design of experiment and other optimization methods (*M. Arun et al., 2021*). The design of an experiment

is a structured and systematic approach used to investigate and understand the relationship between input variables and their effect on the output of a process. It is widely used in manufacturing, engineering, and research and development industries to optimize and improve product and process design. In this thesis, DOE will be used to investigate the factors influencing a specific process and their corresponding effects. This methodical approach enables a detailed analysis of the interplay between multiple variables and their impact on the outcome.

By systematically running experiments for the input factors and observing the resulting responses, DOE reveals underlying patterns, relationships, and optimal conditions. DOE technique helps to streamline the experimentation process by minimizing the number and frequency of experiments needed to achieve meaningful results. *Gowthama et al. (2022)* state that by strategically designing experiments, researchers can maximize the information gathered while reducing the number of trials, thereby saving time, resources, and effort (*Joel et al., 2022*).

The Taguchi Method is an analytical and robust optimization approach in AWJM, emphasizing robust parameter design and noise reduction. Taguchi designs, such as orthogonal arrays, efficiently explore parameter spaces while requiring fewer experimental runs (*Deb, 2024*). The Taguchi Method ensures stable and reliable process performance in AWJM applications by identifying parameter settings that are less sensitive to variations and disturbances.

A comparison of optimization techniques in Abrasive Water Jet Machining (AWJM) studies reveals a variety of methodologies aimed at improving process efficiency and effectiveness. While the Genetic Algorithm (Çetin, 2021) excels in tackling complex, nonlinear optimization problems, Response Surface Methodology (*Nabavi et al., 2022*) provides insights into parameter interactions. However, the Taguchi Method is particularly well-suited for AWJM because it emphasizes robust parameter design and noise reduction. Taguchi designs, such as

orthogonal arrays, efficiently explore parameter spaces with fewer experimental runs, making it a more efficient approach. ANOVA analysis helps identify the primary independent process parameters significantly impacting the responses (*Gangadharan et al., 2022a*). Also, the Taguchi Method's focus on stability and reliability ensures the identification of parameter settings that are less sensitive to process variations, which is relevant in AWJM's dynamic environment.

The simplicity and statistical analysis capabilities of the Taguchi Method also make it accessible and reliable, providing researchers with quantifiable optimization results. Therefore, leveraging the Taguchi Method in AWJM studies offers an efficient, robust, and statistically sound approach to process optimization. However, one limitation of employing the Taguchi methodology is its focus on single-response optimization. This study's three significant output responses—kerf angle, surface roughness, and material removal rate—must be simultaneously optimized, challenging traditional Taguchi optimization approaches.

2.6.2 Taguchi Grey Relational Analysis Optimization

Recent literature has increasingly recognized the potential of combining Taguchi methodology with Grey Relational Analysis (GRA) for optimization in various fields. Unlike traditional Taguchi optimization, which primarily focuses on single-response optimization, the integration of GRA allows for the simultaneous optimization of multiple responses. This approach offers several advantages, including enhanced robustness in handling complex machining processes with multiple interrelated variables and the ability to consider interactions between different responses (*Kehinde, 2021*). When optimizing process parameters for multi-response characteristics, GRA is the most reliable and consistent method, outperforming other techniques like regression, fuzzy logic, and Artificial Neural Network models (*Senthilkumar et al., 2020*). GRA's ability to efficiently explore the vast output responses makes it ideal for

optimizing process parameters involving multiple conflicting objectives. This study investigates three response variables: surface roughness, kerf angle, and material removal rate. The goal is to minimize surface roughness (Ra) and kerf angle while maximizing material removal rate (MRR). Studies have shown that Taguchi GRA optimization outperforms traditional Taguchi optimization in scenarios with multiple response variables, offering improved settings to optimize surface quality (Canbolat et al., 2019).

The review of existing literature discovered that no research had been conducted on aluminum 6061-T6 and 1020 carbon steel with three varied thicknesses for each. This study focused on investigating the impact of different material thicknesses on the quality of the responses. Individual responses were optimized using the Taguchi experiment design, and the findings were compared with Grey Relational Analysis (GRA), which simultaneously optimized response variables. Main effect plots and ANOVA were utilized to explore the impact of these parameters on the responses. Also, a validation test was carried out to confirm the accuracy of the optimization model generated using Taguchi-Grey Relational Analysis.

CHAPTER 3: METHODOLOGY

The research methodology employed in this study is experimental and utilizes two prominent optimization techniques: Taguchi design of experiment and Grey Relational Analysis (GRA). Taguchi orthogonal array was generated to systematically explore the effects of process parameters on machining outcomes, encompassing a total of 27 experimental runs. These experimental runs were conducted specifically for the two metals under investigation, namely aluminum and carbon steel. Through this experimental setup, the study aimed to comprehensively evaluate the influence of various process parameters on machining performance and quality for aluminum and carbon steel materials.

3.1 Material Selection

The two materials used in this study are aluminum 6061-T6 and 1020 carbon steel, which were chosen for the experiment due to their widespread use in various industries. These materials represent common choices for manufacturing components and structures, making them relevant for studying abrasive water jet machining (AWJM) parameters (*Tisza & Czinege, 2018*). Aluminum 6061-T6 and 1020 carbon steel were selected with varying thicknesses to investigate their response to different machining conditions.

Aluminum 6061-T6 is known for its lightweight properties, corrosion resistance, and ease of machining, making it a popular choice in the aerospace, automotive, and train industries *(Gómora et al., 2017*). 1020 Carbon steel, on the other hand, is valued for its strength, durability, and versatility, making it widely used in machinery, infrastructure, and manufacturing applications (*Silva et al., 2019*). The selection of materials with different thicknesses allows for a comprehensive analysis of how surface roughness is affected by varying material properties and

machining parameters. By studying the response of aluminum and carbon steel to different input parameters, such as water pressure, abrasive flow rate, and standoff distance, insights can be gained into optimizing AWJM processes for these materials across a range of thicknesses.

3.2 Machine (WARD Jet -A-0612)

The experiments were performed using the WARDJet A-0612 AWJM machine, known for its high-pressure capabilities, as shown in Figure. Table 1 presents some of the fixed variables of the AWJ machine used for the experiment:

Table 1. *WARDJet Machine Specification*

Parameters	Specification
Diameter of nozzle	0.040 inches
Diameter of the orifice	0.014 inches
Abrasive	Garnet
Jet impact angle	90 degrees
Size of the abrasive	80 mesh
Maximum pressure	413.17 MPa
Traverse speed	1270 mm/min

Figure 4. *WARDJet A-0612*

3.2.1 System Software

Two software programs are relevant when operating the WARDJet machine, namely WARDCAM, proprietary software by WARDJet for the cutting application. This study used it to vary the three traverse speed levels and the cutting paths. MOVE controls the cutting head (Nozzle) and the pump based on the specific water pressure. Figure 5 illustrates the post-processing of the experimental design, which helped to vary the traverse speed based on the

selected three levels and includes the material types and their thicknesses. Based on the experiments, the tool path was manually created to ensure consistency in the machining process.

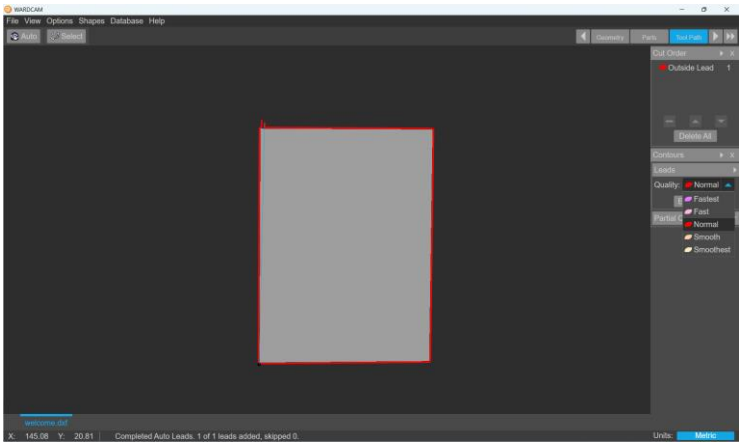

Figure 5. *WARDCAM Interface - WARDDJet*

The MOVE software was utilized to import Computer-Aided Design (CAD) for all experimental procedures. The software controls the input factors such as pressure and standoff distance. Meanwhile, the abrasive flow rate was manually determined using the scale on the abrasive hopper. Figure 6 depicts the MOVE interface with the imported design ready for machining.

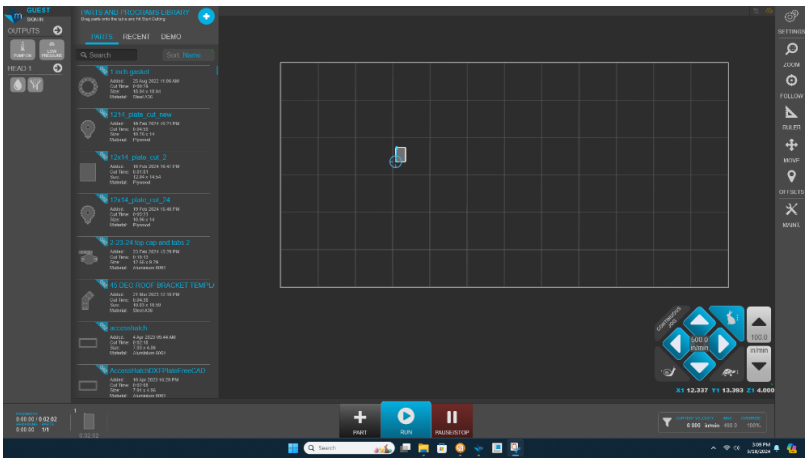

Figure 6. *MOVE Interface - WARDJet*

3.3 Identification of Key Process Parameters

The selection of the five parameters for this study was informed by a comprehensive review of previous research and the AWJM configuration, which identified four commonly used process parameters in abrasive water jet machining (AWJM): water pressure, abrasive flow rate, traverse speed, and standoff distance. These parameters have been widely acknowledged as pivotal in AWJM, as they significantly influence the machining process and the resulting surface finish *(Llanto et al., 2021b*). However, an additional input parameter that has received comparatively less attention is the material thickness. Including material thickness in this study expands the scope of investigated factors likely to influence the output response, specifically surface roughness. While the established parameters play crucial roles in AWJM, exploring the impact of material thickness aims to contribute to a more thorough understanding of the machining process and enhance the overall optimization strategies.

Material thickness was considered a fifth parameter, and this study can provide insights into how the thickness of the material being machined affects the surface roughness, which is a critical aspect of AWJM. This information can be used to optimize the machining process for specific materials and thicknesses, leading to improved surface finishes and reduced material waste. Moreover, the investigation of material thickness as a process parameter can help to identify the optimal thickness range for a given application, which can help minimize stress concentration in manufacturing and improve the overall efficiency of the machining process. In applications where the machined material is subjected to high levels of stress and strain, such as in the aerospace and automotive industries, this consideration holds particular importance.

3.3.1 Selection of Factor Levels

This study systematically examined the effects of critical parameters on abrasive water jet machining (AWJM) by carefully selecting three distinct levels for each parameter. The levels

were chosen based on material thickness and previous project machining experience. Each factor was categorized into low, medium, and high levels for both metals to ensure a thorough investigation of their properties.

Table 2. *Input Factors and Their Levels for Aluminum 6061 T6*

		Levels		
Factors(x)	**Unit**	**1**	**2**	**3**
Pressure	MPa	344	361	379
Abrasive flowrate	g/min	45	101	127
Traverse speed	mm/min	76.2	101.6	127
Standoff Distance	mm	2	2.5	3
Material Thickness	mm	1.016	3.175	4.826

Table 3. *Input Factors and Their Levels for 1020 Carbon Steel*

		Levels		
Factors(x)	**Unit**	**1**	**2**	**3**
Pressure	MPa	372	386	399
Abrasive flowrate	g/min	218	227	250
Traverse speed	mm/min	25.40	50.80	76.20
Standoff Distance	mm	2	2.5	3
Material Thickness	mm	6.350	9.525	12.700

Tables 2 and 3 show the various levels for each aluminum and carbon steel input factor.

3.3.2 Determination of Response Variables

In determining response variables, the focus was on key metrics such as surface roughness (Ra), material removal rate (MRR), and kerf angle. The Ra value is a commonly employed metric for evaluating surface roughness, as it represents the average distance between the peaks and valleys of the profile (*Hidalgo et al., 2018*). Surface roughness (Ra) explicitly represents the arithmetic mean deviation of the surface profile from the mean line, providing crucial insights into the quality of the machined surface (*Edriys et al., 2020*). The material removal rate measures the amount of material removed per unit of time during the machining

process, reflecting the efficiency and effectiveness of the AWJM operation *(Kant & Dhami, 2021*). kerf angle represents the angle formed by the sides of the cut made by the abrasive water jet. It indicates the deviation of the cut from a perpendicular orientation to the workpiece surface. The kerf angle is a critical parameter as it directly influences the machined part's dimensional accuracy, surface finish, and quality (*Shastri et al., 2021*). A smaller kerf angle typically results in a more precise cut with finer details. In comparison, a larger kerf angle may lead to tapering or widening of the cut, affecting the part's geometry and overall quality. These three responses are calculated using the following relations:

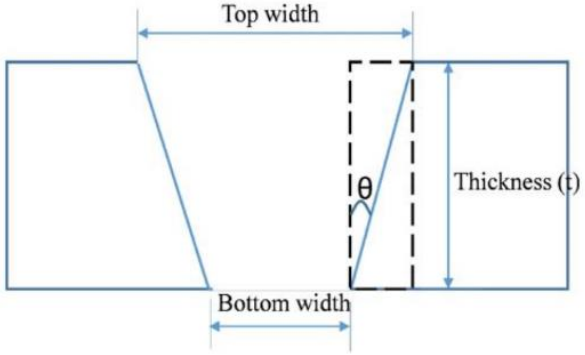

Figure 7. *Representation of the kerf Geometry(Fuse et al., 2021)*

$$MRR = \left(\frac{W_t + W_b}{2}\right) x\ T\ x\ T_s \quad (1)$$

$$Kerf\ angle\ (\Theta) = tan^{-1}\frac{(W_t - W_b)}{2\ x\ T} \quad (2)$$

Where W_t , W_b , T, T_s represents upper kerf width (mm), bottom kerf width (mm), thickness (mm) and the traverse speed (mm/min) (Edriys et al., 2020), (Kant & Dhami, 2021).

The measurement of these output responses is paramount for several reasons. Surface roughness directly impacts machined components' functional performance and aesthetics in various industries, especially welding. Understanding and optimizing surface roughness can enhance

product quality, reduce post-processing requirements, and ensure compliance with design specifications.

The Ra was measured using the SPI surface roughness tester II and a 3D printed fixture to hold the metals in place, while the measurements were taken in Figure 8 and Figure 9, respectively. MRR is an indicator of machining efficiency and productivity. Manufacturers can optimize production processes, minimize costs, and maximize throughput by accurately measuring material removal rates where the calculation was performed using equation 1. Lastly, kerf width directly affects dimensional accuracy and part tolerances. Controlling kerf width is essential for achieving precise cuts, minimizing material wastage, and ensuring the machined part's dimensional integrity(tolerance). Equation 2 was used to attain the Kerf angle for each run.

Figure 8. *SPI Tester II Surface Roughness*

3.4 Experimental Design

The Taguchi orthogonal array is a particular type of experimental design that uses a limited number of experiments to identify the optimal settings for a process or product. It is a set of experimental runs carefully chosen to provide maximum information about the factors being studied(Kusnurkar & Singh, 2019). The Taguchi orthogonal array was generated for the setup

L27 in Tables 4 and 5, which creates a 27 experimental matrix of all the factors and levels to evaluate the impact of the input factors on the output responses for aluminum and carbon steel. The OA for all 27 experiments was run to measure the output responses for the two metal types.

Table 4. *Taguchi OA for 1020 Carbon Steel*

Exp. No.	Water pressure (MPa)	Abrasive Flowrate (g/min)	Traverse Speed (mm/min)	Standoff Distance (mm)	Material Thickness (mm)
1	372	218	25.4	2	6.35
2	372	218	25.4	2	9.525
3	372	218	25.4	2	12.7
4	372	227	50.8	2.5	6.35
5	372	227	50.8	2.5	9.525
6	372	227	50.8	2.5	12.7
7	372	250	76.2	3	6.35
8	372	250	76.2	3	9.525
9	372	250	76.2	3	12.7
10	386	218	50.8	3	6.35
11	386	218	50.8	3	9.525
12	386	218	50.8	3	12.7
13	386	227	76.2	2	6.35
14	386	227	76.2	2	9.525
15	386	227	76.2	2	12.7
16	386	250	25.4	2.5	6.35
17	386	250	25.4	2.5	9.525
18	386	250	25.4	2.5	12.7
19	399	218	76.2	2.5	6.35
20	399	218	76.2	2.5	9.525
21	399	218	76.2	2.5	12.7
22	399	227	25.4	3	6.35
23	399	227	25.4	3	9.525
24	399	227	25.4	3	12.7
25	399	250	50.8	2	6.35
26	399	250	50.8	2	9.525
27	399	250	50.8	2	12.7

Table 5. *Taguchi OA for Aluminum 6061-T6*

Exp. No.	Water pressure (MPa)	Abrasive Flowrate (g/min)	Traverse Speed (mm/min)	Standoff Distance (mm)	Material Thickness (mm)
1	344	45	76.2	2	1.016
2	344	45	76.2	2	3.175
3	344	45	76.2	2	4.826
4	344	101	101.6	2.5	1.016
5	344	101	101.6	2.5	3.175
6	344	101	101.6	2.5	4.826
7	344	127	127	3	1.016
8	344	127	127	3	3.175
9	344	127	127	3	4.826
10	361	45	101.6	3	1.016
11	361	45	101.6	3	3.175
12	361	45	101.6	3	4.826
13	361	101	127	2	1.016
14	361	101	127	2	3.175
15	361	101	127	2	4.826
16	361	127	76.2	2.5	1.016
17	361	127	76.2	2.5	3.175
18	361	127	76.2	2.5	4.826
19	379	45	127	2.5	1.016
20	379	45	127	2.5	3.175
21	379	45	127	2.5	4.826
22	379	101	76.2	3	1.016
23	379	101	76.2	3	3.175
24	379	101	76.2	3	4.826
25	379	127	101.6	2	1.016
26	379	127	101.6	2	3.175
27	379	127	101.6	2	4.826

3.4.1 Specimen Design

The specimen dimensions illustrated in Figure 9 were created using CREO Parametric, with a length of 2 inches (50.8 mm) and a width of 3 inches (76.2 mm). These dimensions remained consistent across all 27 experiments conducted for three different thicknesses. Each

specimen's design was saved as a DXF extension file and processed in WARDCAM. The file naming convention, such as "Exp x-thickness-traverse speed" (e.g., Exp 1_0.04_76.2), facilitated easy identification of individual files corresponding to each unique combination of experimental parameters.

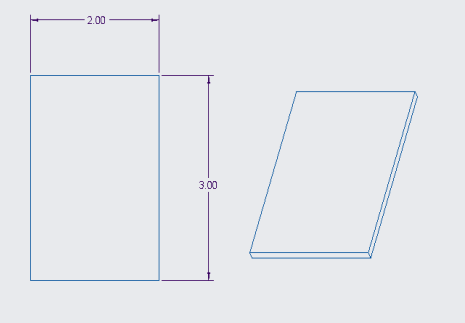

Figure 9. *Specimen Dimension*

3.5 Experimental Setup

Each thickness underwent separate machining to minimize potential sources of error, ensuring accurate results. By machining each thickness individually, the effects of any variations or influences specific to that thickness could be accurately assessed and accounted for in the analysis. This approach enabled meaningful comparisons between different runs and thicknesses, further enhancing the validity of the findings. The standoff distance was consistently maintained for each consecutive run of the same thickness. This consistency in standoff distance ensured that cutting parameters remained constant without having to vary the standoff distance for each thickness. Figure 10 depicts the setup for the experiment.

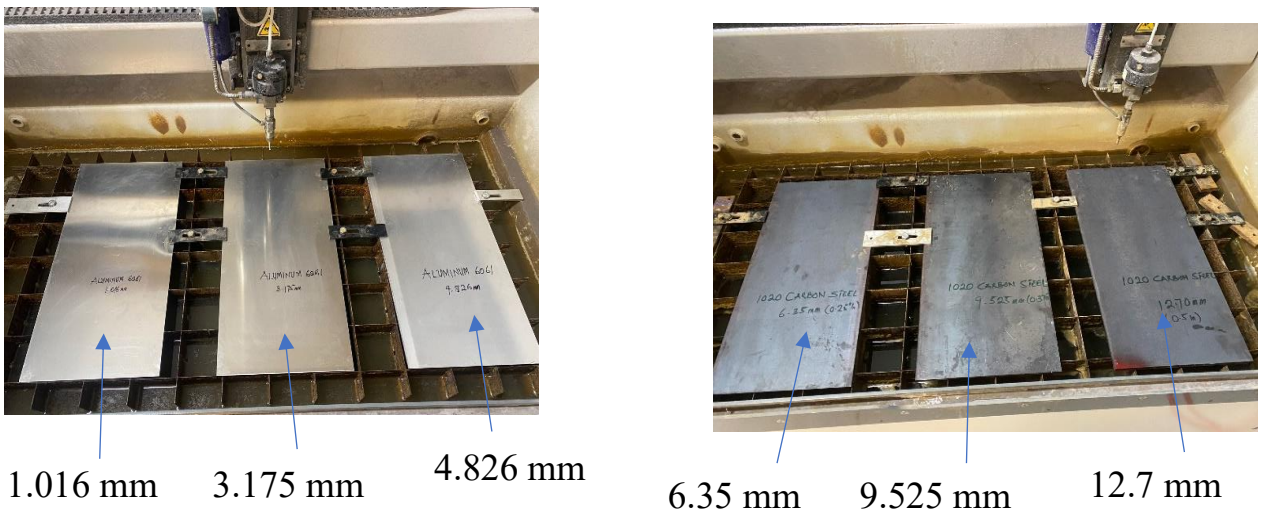

Figure 10. *Setup for the Experimental Runs*

3.5.1 Measured Result for the Output Responses

The Ra responses were measured using the surface roughness texter II Figure 8. The other two output responses, material removal rate and kerf angle, were calculated using equations 1 and 2, respectively. Tables 6 and 7 presented all the results for the 27 experimental runs for each output response.

Table 6. *Measured Responses for Aluminum 6061-T6*

No.	MRR (mm^3/min)	Kerf Angle(degrees)	Surface Roughness Ra(um)
1	5.85	0.20	3.65
2	16.45	0.18	3.68
3	22.80	0.13	4.17
4	8.10	0.03	3.40
5	23.71	0.12	3.70
6	34.57	0.12	3.79
7	9.87	0.08	3.71
8	29.44	0.14	3.75
9	42.90	0.12	3.93
10	7.69	0.14	4.29
11	21.45	0.23	4.56
12	31.87	0.13	4.69
13	9.81	0.17	3.15
14	27.02	0.14	3.75
15	40.76	0.10	4.37
16	6.00	0.03	3.35
17	18.27	0.05	3.51
18	27.58	0.08	3.76
19	9.48	0.14	3.89
20	26.81	0.21	4.01
21	37.39	0.13	4.16
22	6.15	0.20	3.90
23	18.27	0.10	3.92
24	27.03	0.08	4.03
25	8.15	0.06	3.18
26	22.90	0.05	3.32
27	35.55	0.07	4.76

Table 7. *Measured Responses for 1020 Carbon Steel*

No.	MRR (mm3/min)	Kerf Angle(degrees)	Surface Roughness Ra(um)
1	10.00	0.04	3.56
2	15.73	0.04	4.03
3	20.97	0.05	4.75
4	20.65	0.09	3.67
5	30.00	0.08	3.92
6	39.35	0.07	4.88
7	30.97	0.10	3.97
8	42.10	0.10	4.01
9	56.13	0.08	4.81
10	21.13	0.08	3.66
11	31.45	0.07	4.10
12	39.35	0.08	4.56
13	28.79	0.09	3.34
14	43.19	0.09	4.00
15	55.65	0.07	4.66
16	11.05	0.08	3.50
17	16.33	0.05	4.15
18	22.10	0.04	4.44
19	30.00	0.11	3.82
20	42.82	0.10	4.11
21	56.13	0.08	4.89
22	11.13	0.06	3.40
23	16.57	0.07	4.59
24	20.97	0.05	4.78
25	20.48	0.09	3.26
26	30.73	0.07	4.07
27	38.39	0.06	4.39

3.6 Taguchi Design of Experiment

3.6.1 Taguchi Single Response Optimization

This method was adopted to thoroughly assess the significance of each input factor on the output responses. The Signal to Noise (S/N) ratio is a metric used to evaluate the quality of a process input parameters on the response characteristics by converting the data into S/N ratios (*Patel G C et al., 2020*). It identifies the optimal combination of input factors that maximizes the signal (desired output) while minimizing the noise (undesired variation). A higher value of the

S/N ratio indicates substantial parameter stability (*Kant & Dhami, 2021*). Three types of S/N ratios are commonly employed in Taguchi optimization (*Gangadharan et al., 2022a*).

In this study, the focus was narrowed down to just two types of signal-to-noise (S/N) ratios: "smaller is better" and "larger is better," as seen in equations 3 and 4, respectively. This decision was made because it was observed that two of the responses were expected to improve with lower numbers, while the third response was expected to improve with higher numbers. This approach simplified the analysis by concentrating on these specific S/N ratio categories.

Smaller-is-Better (SiB): This S/N ratio is used when the goal is to minimize the response variable (Kerf angle and surface roughness). In this case, a higher S/N ratio indicates better performance (Minimize S/N ratio).

$$S/N_{SiB} = -10\,x\log\left(\sum\left(\frac{y^2}{n}\right)\right) \tag{3}$$

Where y is the response for the given factor level combination, and n is the number of the responses in the factor level combination.

Larger-is-Better (LiB): This S/N ratio is used when the goal is to maximize the response variable (material removal rate). In this case, a higher SN ratio indicates better performance (Maximize S/N ratio).

$$S/N_{LiB} = -10\,x\log\left(\sum\frac{\left(\frac{1}{y^2}\right)}{n}\right) \tag{4}$$

Where y is the response for the given factor level combination, and n is the number of responses in the factor level combination.

3.6.2 Analysis of Variance (ANOVA)

The subsequent phase of the analysis is the ANOVA, which explains the significance of the process input factors on the various responses such as the surface roughness, kerf angle, and the material removal rate (*Kant & Dhami, 2021*). The study analyzed the impact of various input factors on output responses using a significance level of 5% and a confidence level of 95%. The analysis involved calculating statistical measures such as the Sum of Squares, Square Means, P-values, and F-values, which provided insights into the influence of different input factors on the output parameters. Specifically, the P-value was used to assess the significance of each input factor on the output responses. In most research, a significant level of 5%, denoted by the alpha value of 0.05, is considered the threshold for determining a direct influence. If the P-value for a particular input factor is less than this threshold, it indicates a direct and statistically significant impact of that factor on the output responses (*Gangadharan et al., 2022a*).

The main effect plots of the S/N ratio illustrate the optimal factor-level combinations for a given response. By displaying the mean S/N ratio at each level of the input factors, these plots assist in selecting the most suitable settings to achieve optimal results (*Fuse et al., 2021*).

3.7 Multi-Response Optimization

3.7.1 Taguchi – Grey Relational Analysis

Traditional optimization methods, such as the Taguchi method, focus on improving a single response, neglecting the interdependencies between other responses (*Senthil Kumar et al., 2020*). This limitation can lead to suboptimal solutions and hinder the system's performance. The Grey-Taguchi method overcomes this limitation by incorporating the concept of grey relational analysis, which considers the interconnectedness between multiple responses (*Joel & Jeyapoovan, 2021*). Real-world engineering applications commonly involve multiple dependent variables, making direct optimization using the Taguchi method impractical. To overcome this

challenge, integrating Grey Relational Analysis (GRA) with the Taguchi method introduces a novel methodology for multi-parameter optimization called the Grey-Taguchi method.

3.7.2 Taguchi-Grey Relational Analysis Model

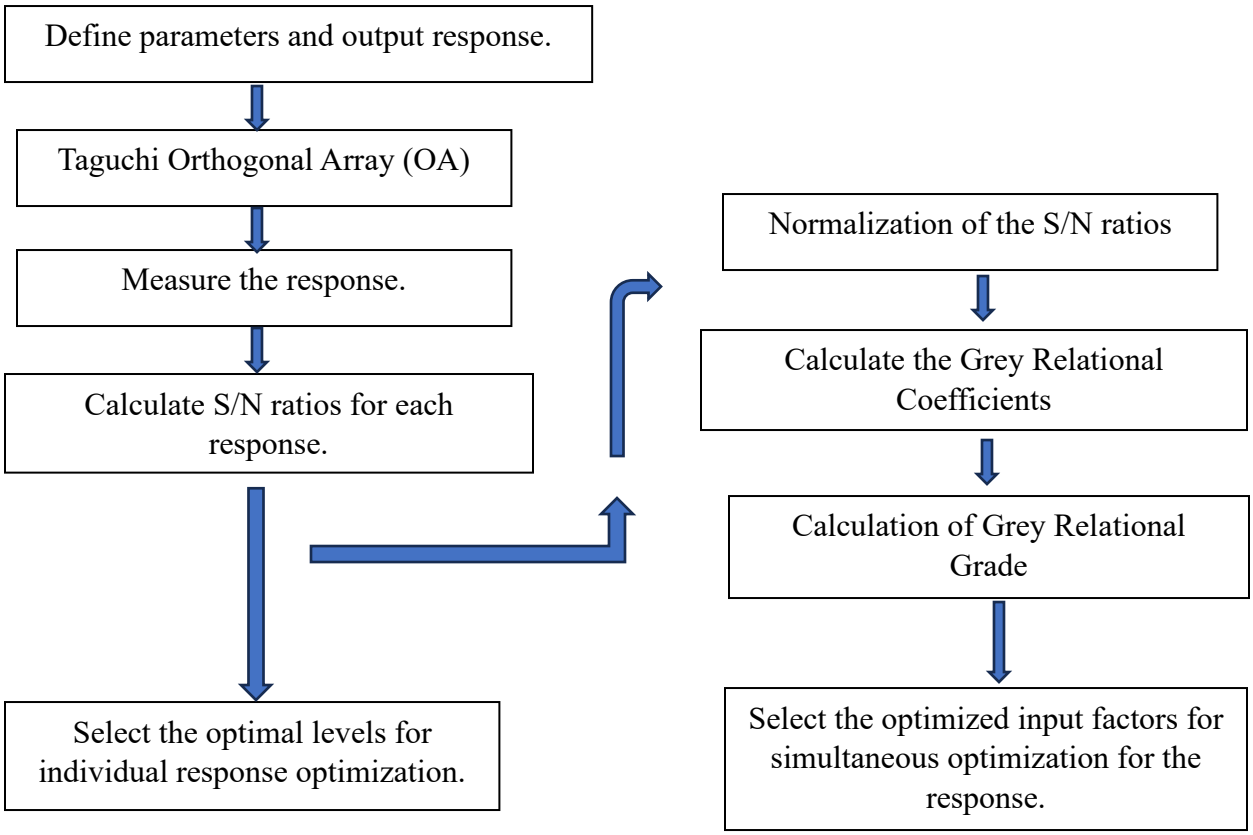

Figure 11. *Flow chart for the Taguchi Grey Relational Optimization (Qazi et al., 2020)*

After the Taguchi single response is achieved, the GRA is implemented after calculating the signal-to-noise ratio. In the initial phase of Grey Relational Analysis, the process begins with grey relational formation, where experimental outcomes are standardized to a scale ranging from 0 to 1 to accommodate differences in measurement units (*Bangphan & Bangphan, 2014*). The various equations 5 and 6 were used to normalize the S/N ratio based on the criteria: larger is better and smaller is better, respectively *(Nayakappa, 2015*).

For larger is better the quality characteristics for MRR, the normalization values are given by:

$$Y_i(r) = \left(\frac{y_{\max(r)} - y_{i(r)}}{y_{\max(r)} - y_{\min(r)}}\right) \quad (5)$$

For smaller is better the quality characteristics for surface roughness and kerf angle, the normalization values are given by:

$$Y_i(r) = \left(\frac{y_{i(r)} - y_{min}}{y_{\max(r)} - y_{\min(r)}}\right) \quad (6)$$

Where $Y_i(r)$ represent the normalized S/N ratios for each response variable, whereas $y_{\max(r)}$ and $y_{\min(r)}$ are the largest and smallest values of $Y_i(r)$ for the i^{th} number of experimental runs respectively. There are three output responses to be optimized: Ra, Θ and MRR: therefore r = 3. The following computation is the deviation sequence, which is calculated using equation 7.

$$\Delta_{i(r)} = \left| Y_{0(r)} - y_{i(r)} \right| \quad (7)$$

The deviation sequence is determined by calculating the absolute difference between the reference sequence $Y_{0(r)}$ and the comparative sequences $y_{i(r)}$. The distinguishing coefficient (ζ) is assigned a value between 0 and 1, typically set at 0.5, as commonly observed to yield optimal results in research. Grey Relational Grade (GRG) offers insights into the correlation strength among experimental runs, calculated through the weighted average of their respective Grey Relational Coefficients (GRCs) using equation 8 across all experiments (*Qazi et al., 2020*).

$$GRC = \frac{\Delta_{\min(r)} + \zeta \Delta_{\max(r)}}{\Delta_{0(r)} + \zeta \Delta_{\max(r)}} \quad (8)$$

Where $\Delta_{\min}$ and $\Delta_{\max}$ are the respective the minimum and maximum vales of the deviation sequence for each response. The grey relational grade is calculated using the equation below.

$$GRG = \frac{1}{n}\sum_{r=1}^{n} w_r \xi\,(r) \tag{9}$$

Where ξ(r) is the GRC for each response for the entire run, n is the number of quality responses, and w_r is the weight of r^{th}. The total weight for each response sums up to 1. However, the same weight of 0.333 was used for all three responses.

$$\gamma_{predicted} = \gamma_m + \sum_{r=1}^{n} \gamma_0 - \gamma_m \tag{10}$$

γ_0 indicates the highest average Grey Relational Grade (GRG) achieved when factors are at their optimal levels, while γ_m represents the mean GRG across all levels of factors *(Obinna Anayo et al., 2022*).

The highest Grey Relational Grade signifies the most robust relationship or correlation among response variables in Grey Relational Analysis. It is represented by a single numeric value, reflecting the overall performance of the optimal input settings in the analysis. The GRG value is further fine-tuned in response to the other input factors through Minitab. Generating a response table and conducting ANOVA are involved in identifying the optimal settings and significant factors that collectively influence all the responses (*Girish et al., 2019*).

CHAPTER 4: RESULTS

4.1 Single Response Optimization- Taguchi

The analysis for each output response shows the significance of each input factor on the response variable using analysis of variance and the main effect plot. The statistical tool used for the study is Minitab, and the analysis was performed at a 95 % confidence level. Notably, a p-value less than 0.005 shows the significance of the input factors (*Ogbonna et al., 2023*). The results include the response table, analysis of variance (ANOVA), main effect plot, and the predicted plots for each output response (surface roughness, kerf angle, and material removal rate).

4.2 Optimization Analysis for Aluminum 6061-T6

Taguchi utilizes signal-to-noise (S/N) ratio, as a performance parameter to gauge deviation from desired outcomes. Higher S/N ratios are preferred for minimizing the impact of uncontrolled factors, aiming to reduce noise, and identifying the optimal settings *(Padhy & Singh, 2020*). The S/N ratio reflects the sensitivity of the response to variation, where the main effect for the S/N ratio with a higher S/N ratio indicates that a slight change in the input factor can lead to a more significant change in the output response.

4.2.1 Surface Roughness (Ra)

The response in Table 8 shows the critical factor that highly influences the surface roughness response based on the signal-to-noise ratio. Material thickness was ranked as the input factor that significantly impacts Ra, followed by abrasive flow rate and standoff distance, which intuitively confirms their impact on surface quality after machining. Since a smaller Ra value indicates a good surface quality, the signal-to-noise ratio criteria for Ra is smaller is better. The delta value is the difference between the largest and the smallest S/N ratio. The ranking gives a general picture of the factors that impact the response variable, which is the surface roughness;

however, ANOVA gives detailed information about how each input factor contributes to the output response based on the p values.

Table 8. *Response Table for S/N Ratios – Surface Roughness (Ra)*

Level	Water pressure (MPa)	Abrasive Flowrate(g/min)	Traverse Speed(mm/min)	Standoff Distance(mm)	Material Thickness(mm)
1	**-11.48**	-12.27	**-11.52**	-11.43	**-11.08**
2	-11.82	-11.51	-11.83	**-11.41**	-11.56
3	-11.75	**-11.26**	-11.70	-12.20	-12.40
Delta	0.35	1.01	0.32	0.79	1.33
Rank	4	2	5	3	1

Note. Smaller is better (S/N ratios).

From the main effect plot for S/N ratios from Figure 12, the optimal setting comes from the high signal-to-noise ratio. Wp1-Af3-Ts1-Sd2-Mt1 is the setting code representing water pressure at level 1, abrasive flow at level 3, traverse speed at level 1, standoff distance at level 2, and Material thickness at level 1. Representing 344 MPa,127 g/min,76.20 mm/min,2.50 mm and 1.016 mm respectively.

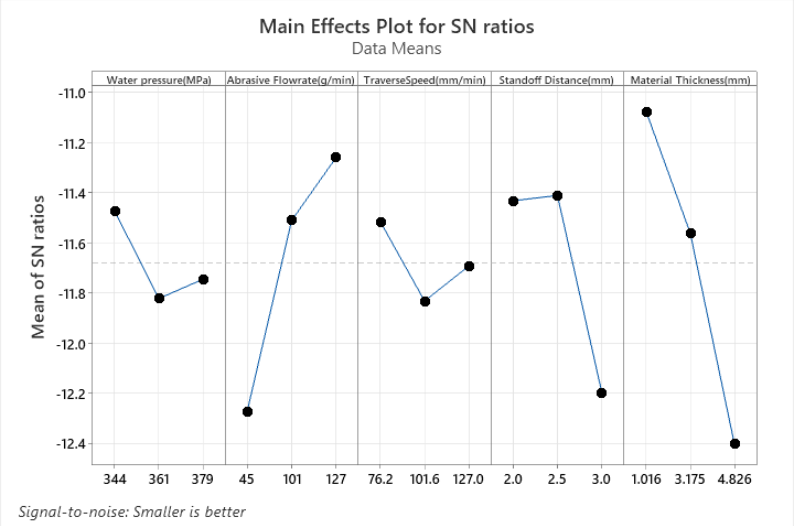

Figure 12. *Main Effect Plot for the S/N Ratios – Surface Roughness (Ra)*

Analysis of variance (ANOVA) gave much insight into the input factors and their significance to the output response. The confidence level for this study is 95%, with a significance level of 0.05. Therefore, any p-value less than 0.05 is significant to the response where the response here is Ra. The input factors that highly influence the Ra are abrasive flow rate, standoff distance, and material thickness, which have p values less than 0.05.

Table 9. *Analysis of Variance for Surface Roughness (Ra)*

Source	DF	Seq SS	Contribution	Adj SS	Adj MS	F-Value	P-Value
Water pressure (MPa)	2	0.1659	3.40%	0.1659	0.08296	1.00	0.390
Abrasive Flowrate(g/min)	2	0.9589	19.67%	0.9589	0.47945	5.77	**0.013**
Traverse Speed(mm/min)	2	0.1424	2.92%	0.1424	0.07120	0.86	0.443
Standoff Distance(mm)	2	0.6910	14.17%	0.6910	0.34549	4.16	**0.035**
Material Thickness(mm)	2	1.5881	32.57%	1.5881	0.79406	9.56	**0.002**
Error	16	1.3296	27.27%	1.3296	0.08310		
Total	26	4.8759	100.00%				

Note. Confidence level of 95%

The graph in Figure 13 shows the actual response value for Ra and the predicted result for all five input factors and three input factors. The three predicted regression models were established after eliminating the non-significant factors from the model. Evidently, there is a trend pattern for the results, and the actual results follow this trend closely. The three and five predicted models show that having more factors gives better output response results than having fewer factors.

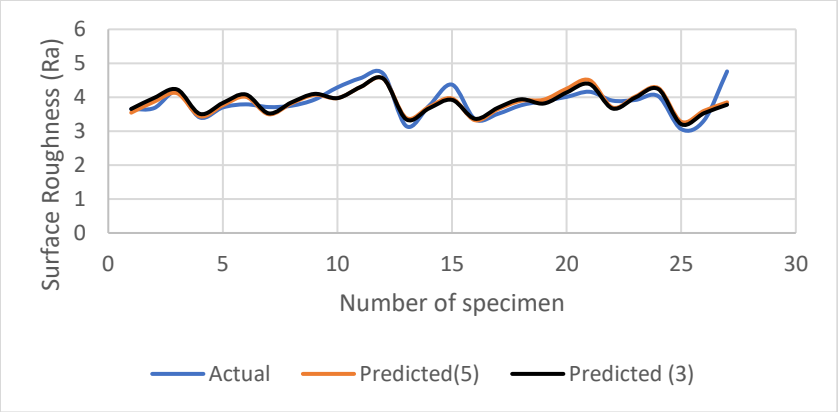

Figure 13. *Actual vs. Predicted data for 5 and 3 Factors Respectively*

4.2.2 Kerf Angle

The abrasive flow rate was ranked as the significant control factor to the kerf angle, which is the angular deviation between the top and bottom kerf widths. The top cut is wider than the bottom based on the waterjet force cutting through the metal, whereas the top cut tends to experience the total water jet energy. However, the water's energy is dissipated at the bottom, resulting in minor cuts. The amount of abrasive present in the water determines how much shear through the metal happens, leading to the kerf angle. Other factors are also influential to the kerf angle, Like the standoff distance, which affects the shape of the water stream before encountering the metal. However, ANOVA Table 10 further analyzes this factor and presents their contribution to kerf angle.

Table 10. *Response Table for S/N Ratios – Kerf Angle*

Level	Water pressure (MPa)	Abrasive Flowrate(g/min)	Traverse Speed(mm/min)	Standoff Distance(mm)	Material Thickness(mm)
1	19.01	15.85	20.29	19.20	**20.68**
2	**19.92**	19.59	**21.04**	**21.73**	18.45
3	19.86	**23.37**	17.48	17.87	19.68
Delta	0.91	7.52	3.56	3.86	2.23
Rank	5	1	3	2	4

Note. Smaller is better (S/N ratios)

The optimal setting for single response optimization for kerf angle from Figure 14 shows water pressure at level 2, abrasive flowrate at level 3, traverse speed at level 2, standoff distance at level 2, and material thickness at level 1 (Wp2-Af3-Ts2-Sd2-Mt1). Each level has a corresponding setting value at the bottom of the plot. The Abrasive flowrate shows a steeper slope in the plot, indicating its significant influence on the kerf angle.

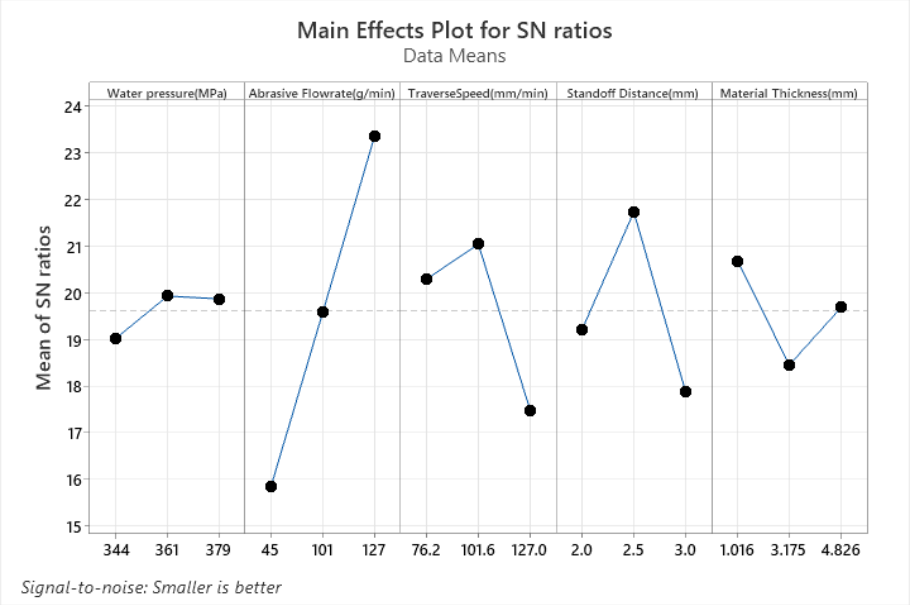

Figure 14. *Main Effect Plot for the S/N Ratios – Kerf Angle*

The response table below for the S/N ratio shows that standoff distance comes after abrasive flowrate for the factors that are significant to the kerf angle; however, from the statistical perspective, the p-value for standoff distance is 0.228, which is greater than the significance of 0.05, and its contribution to the variation is about 7.07%. ANOVA confirms that the kerf angle variation's abrasive flow rate is statistically significant.

Table 11. *Analysis of Variance for Kerf Angle*

Source	DF	Seq SS	Contribution	Adj SS	Adj MS	F-Value	P-Value
Water pressure (MPa)	2	0.000535	0.68%	0.000535	0.000268	0.16	0.856
Abrasive Flowrate(g/min)	2	0.036022	45.97%	0.036022	0.018011	10.56	**0.001**
Traverse Speed(mm/min)	2	0.005150	6.57%	0.005150	0.002575	1.51	0.251
Standoff Distance(mm)	2	0.005540	7.07%	0.005540	0.002770	1.62	0.228
Material Thickness(mm)	2	0.003814	4.87%	0.003814	0.001907	1.12	0.351
Error	16	0.027302	34.84%	0.027302	0.001706		
Total	26	0.078363	100.00%				

Note. Confidence level of 95%

In Figure 15, the actual and predicted models for kerf angle show irregularities in the trend. The actual (experimental) model shows relatively low kerf angles of 0.03 degrees for experiments 4 and 16. On the other hand, there were some high values in the same experimental run, which were more than the predicted values for all five input factors and one input factor. Investigation shows that the kerf angle is sensitive to the material thickness. Based on the input factor level constraints, material thickness can reduce the angular deviation between the top and bottom cut of the metal.

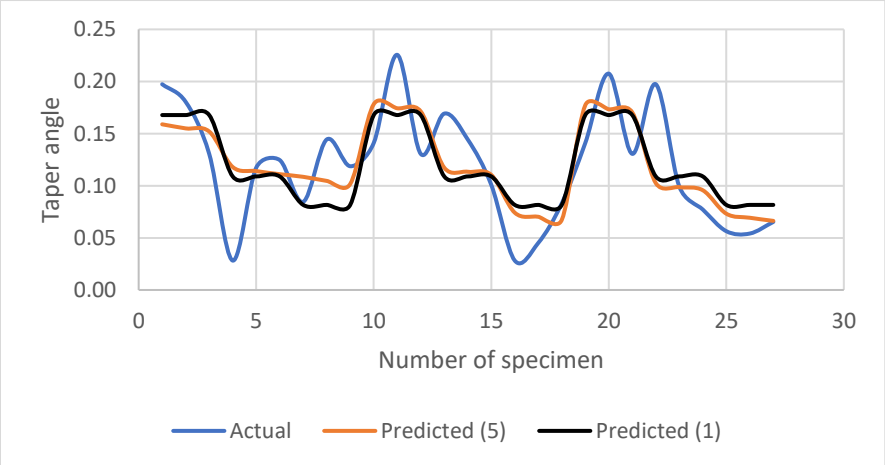

Figure 15. *Actual vs. Predicted data for 5 and 1 Factor Respectively*

4.2.3 Material Removal Rate (MRR)

Material thickness was obviously the main input factor influencing the amount of material removed per unit time, followed by the traverse speed, which is the speed at which the nozzle head moves over the metal. These two factors are paramount to the MRR mathematical equation, where the removed material volume is multiplied by the material thickness and nozzle speed (traverse speed). The criteria for Material Removal Rate (MRR) analysis is "the larger, the better" regarding the S/N ratio, as increased material removal is desirable.

Table 12. *Response Table for S/N Ratios - MRR*

Level	Water pressure (MPa)	Abrasive Flowrate(g/min)	Traverse Speed(mm/min)	Standoff Distance(mm)	Material Thickness(mm)
1	25.02	24.53	22.90	24.88	17.78
2	24.97	25.20	25.26	25.07	26.97
3	**25.07**	**25.33**	**26.90**	**25.11**	**30.31**
Delta	0.11	0.80	4.01	0.23	12.52
Rank	5	3	2	4	1

Note. Larger is better (S/N ratios)

The three factors shown in the plot in the Figure 16 indicate that the main effect plots for water pressure, abrasive flow rate, and standoff distance are horizontal and parallel to the mean line, meaning there is not much variation coming from these input factors on the response. However, material thickness has a much more significant effect on MRR than traverse speed, as indicated by the slope in the plot and conformed in the response table for the S/N ratio. Wp1-Af3-Ts3-Sd3-Mt3 is the optimal setting to achieve high material removal concerning their levels.

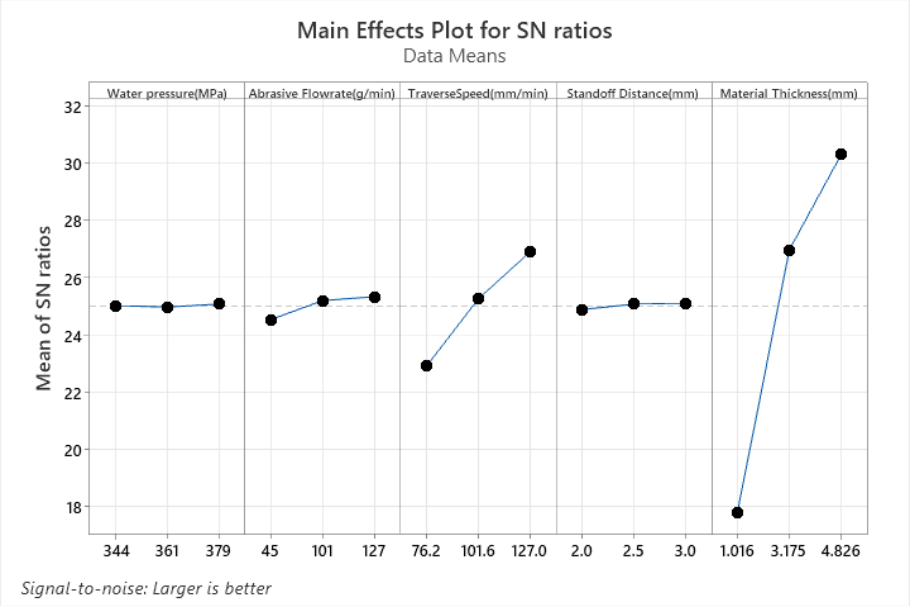

Figure 16. *Main Effect Plot for S/N Ratios - MRR*

Material thickness and standoff distance have p-values less than 0.05, statistically making them significant to MRR. Even though the p-value for both input factors is 0.000, the contribution of material thickness to traverse speed is shown in the ANOVA table. MRR is directly proportional to metal thickness and the speed of the cutting head.

Table 13. *Analysis of Variance for MRR*

Source	DF	Seq SS	Contribution	Adj SS	Adj MS	F-Value	P-Value
Water pressure (MPa)	2	0.59	0.02%	0.59	0.30	0.04	0.957
Abrasive Flowrate(g/min)	2	26.18	0.75%	26.18	13.09	1.95	0.174
Traverse Speed(mm/min)	2	402.86	11.56%	402.86	201.43	30.07	**0.000**
Standoff Distance(mm)	2	1.61	0.05%	1.61	0.81	0.12	0.887
Material Thickness(mm)	2	2947.37	84.55%	2947.37	1473.69	219.98	**0.000**
Error	16	107.19	3.07%	107.19	6.70		
Total	26	3485.81	100.00%				

Note. Confidence level of 95%

This is shown in the models for the actual and predicted results for all factors and the significant input factors (material thickness and traverse speed). All the models follow that same trend where lower and higher data points are for the aluminum thickness of 1.016 mm and 4.826

mm, respectively. Thicker metals will have a large volume of metal removed per unit time during AWJM.

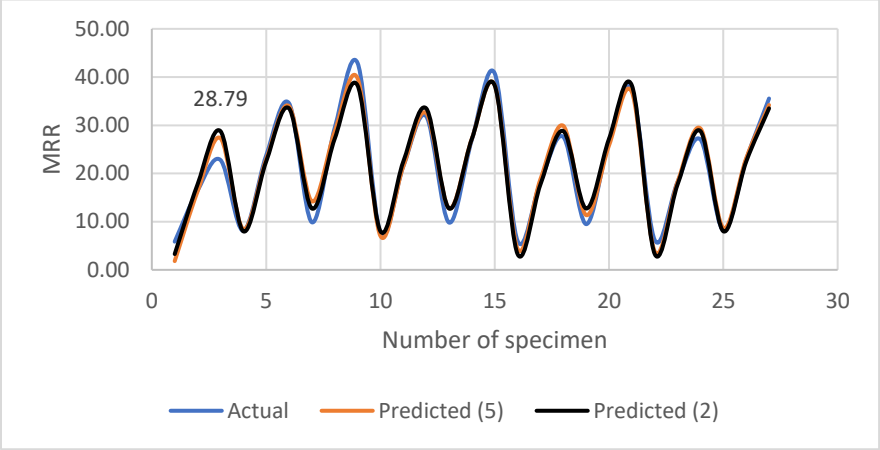

Figure 17. *Actual vs. Predicted data for 5 and 2 Factors Respectively*

4.2.4 Evaluation of Experimental Data

Figure 18 displays the probability plot for all the responses. The data conforms to a normal distribution, which is evident from all the data points falling within the symmetric bell-shaped confidence interval. Additionally, the p-values exceeding 0.05 indicate that the data follows a normal distribution, allowing for further analysis to be conducted confidently.

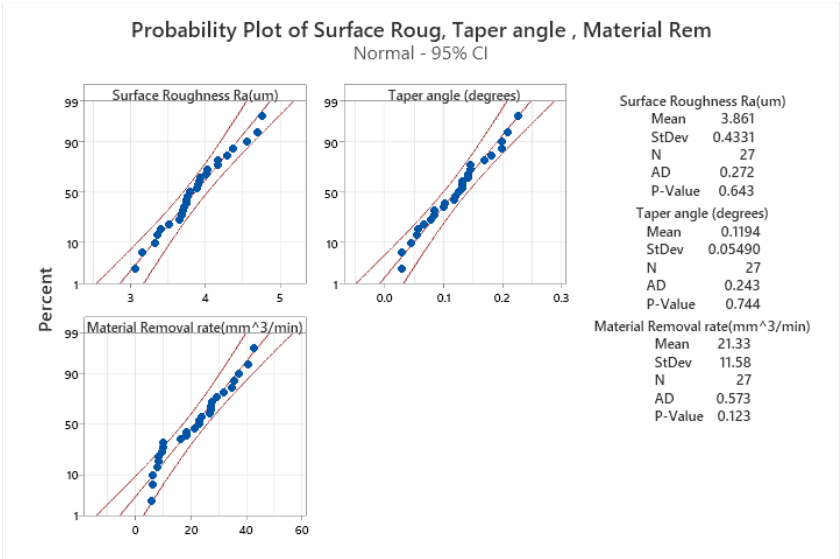

Figure 18. *Probability Plot for the Three Output Responses – Aluminum 6061 – T6*

4.3 Optimization analysis for 1020 Carbon Steel

The 1020 carbon steel was also analyzed based on the same factors and different level settings based on its properties since it is solid and durable compared to aluminum 6061-T6.

4.3.1 Surface Roughness (Ra)

Table 14 shows that the material thickness significantly impacts surface roughness, as indicated by the most considerable delta value (2.36). The rank column indicates the ranking of each factor based on its influence on surface roughness, with a lower rank indicating a more significant impact. Variations in material thickness led to more noticeable changes in surface roughness compared to other factors.

Table 14. *Response Table for S/N Ratios – Surface Roughness (Ra)*

Level	Water pressure (MPa)	Abrasive Flowrate(g/min)	Traverse Speed(mm/min)	Standoff Distance(mm)	Material Thickness(mm)
1	-12.36	-12.34	-12.26	**-11.98**	**-11.05**
2	**-12.09**	-12.25	**-12.10**	-12.31	-12.27
3	-12.27	**-12.13**	-12.36	-12.43	-13.41
Delta	0.28	0.21	0.26	0.44	2.36
Rank	3	5	4	2	1

Note. Smaller is better (S/N ratios)

The plot in Figure 19 reveals that material thickness has the highest rank (1) in influencing surface roughness, indicating its significant impact on the quality of machined surfaces. This finding aligns with the expectation that thicker materials exhibit higher surface roughness due to increased resistance to the abrasive jet. These settings, Wp2-Af3-Ts2-Sd1-Mt1, represent a balance between cutting efficiency and surface finish quality, resulting in the highest S/N ratio and smoother machined surfaces. Also, when it comes to carbon steel, these optimal settings can lead to several benefits, such as reduced surface roughness and improved dimensional accuracy.

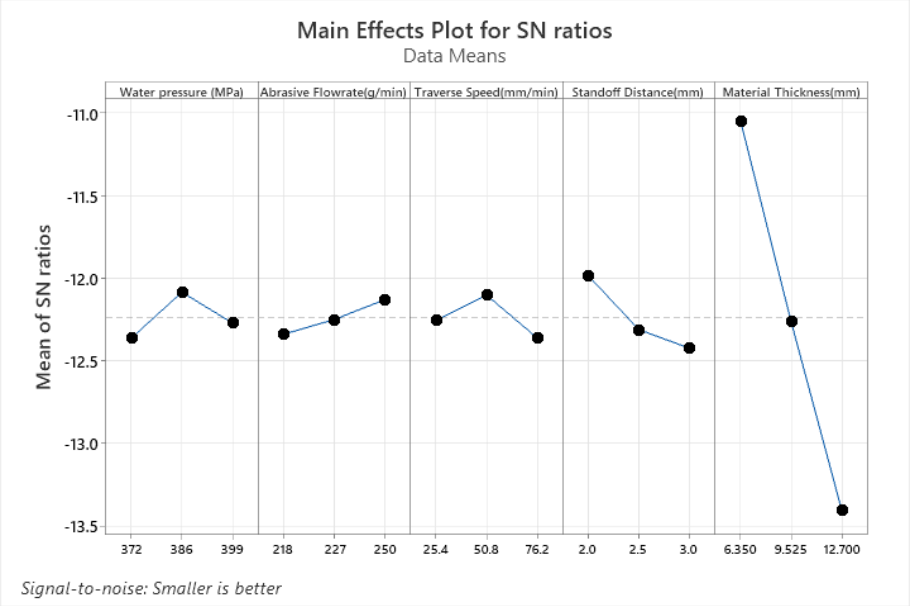

Figure 19. *Main Effect for S/N Ratios – Surface Roughness (Ra)*

The P-value for material thickness is 0.000, indicating a highly significant effect. Material thickness contributes 84.78% of the variance in surface roughness, making it the most influential factor in Table 15. This finding emphasizes the importance of controlling material thickness to achieve the desired surface finish quality.

Table 15. *Analysis of Variance for Surface Roughness (Ra)*

Source	DF	Seq SS	Contribution	Adj SS	Adj MS	F-Value	P-Value
Water pressure (MPa)	2	0.08556	1.31%	0.08556	0.04278	1.15	0.343
Abrasive Flowrate(g/min)	2	0.04599	0.70%	0.04599	0.02299	0.62	0.552
Traverse Speed(mm/min)	2	0.06867	1.05%	0.06867	0.03434	0.92	0.419
Standoff Distance(mm)	2	0.19647	3.01%	0.19647	0.09824	2.63	0.103
Material Thickness(mm)	2	5.53603	84.78%	5.53603	2.76801	74.18	**0.000**
Error	16	0.59704	9.14%	0.59704	0.03731		
Total	26	6.52976	100.00%				

Note. Confidence level of 95%

When comparing the actual surface roughness values obtained under optimal settings with those predicted by the models, a notable trend emerges in Figure 20. The actual surface

roughness values tend to be lower than the predicted values, indicating that the actual data optimal settings consistently outperform the expected outcomes in terms of surface quality.

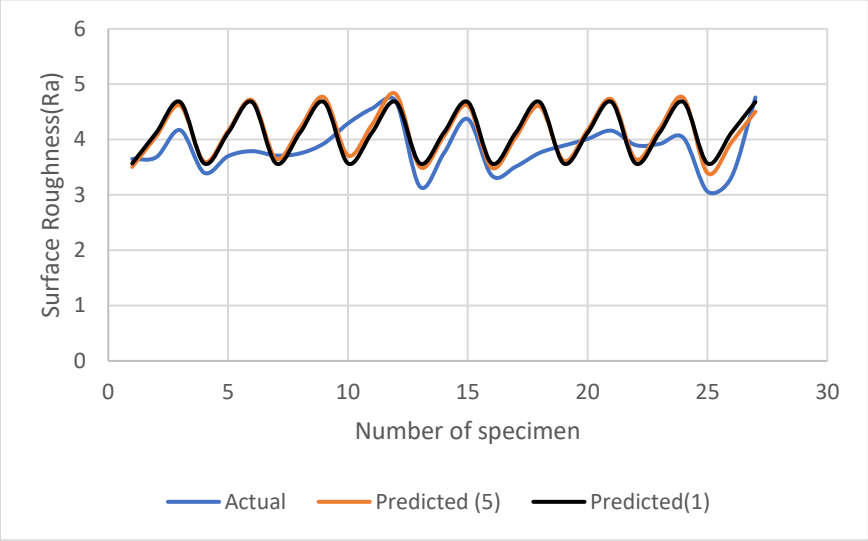

Figure 20. *Actual vs. Predicted data for 5 and 1 Factors Respectively*

4.3.2 Kerf Angle

The S/N ratios indicate that traverse speed significantly impacts the kerf angle, as evidenced by its highest rank (1). A lower S/N ratio implies a better kerf angle. In this case, the higher delta value for traverse speed indicates a substantial improvement in the kerf angle as the speed increases. Adjusting the traverse speed can significantly improve the kerf angle.

Table 16. *Response Table for S/N Ratios – Kerf Angle*

Level	Water pressure (MPa)	Abrasive Flowrate(g/min)	Traverse Speed(mm/min)	Standoff Distance(mm)	Material Thickness(mm)
1	**23.47**	**23.60**	**25.98**	**24.11**	22.17
2	23.30	22.71	22.45	22.51	22.91
3	22.63	23.09	20.97	22.78	**24.33**
Delta	0.84	0.89	5.01	1.60	2.16
Rank	5	4	1	3	2

Note. Smaller is better (S/N ratios)

The main effect plot in Figure 21 reveals that traverse speed exhibits the steepest slope among all factors. This steep slope indicates that small changes in traverse speed result in

significant variations in the kerf angle. Therefore, optimizing traverse speed within the appropriate range is crucial for achieving the desired kerf angle. Based on the main effect plot analysis, the optimal settings for achieving the desired kerf angle are Wp1-Af1-Ts1-Sd1-M3.

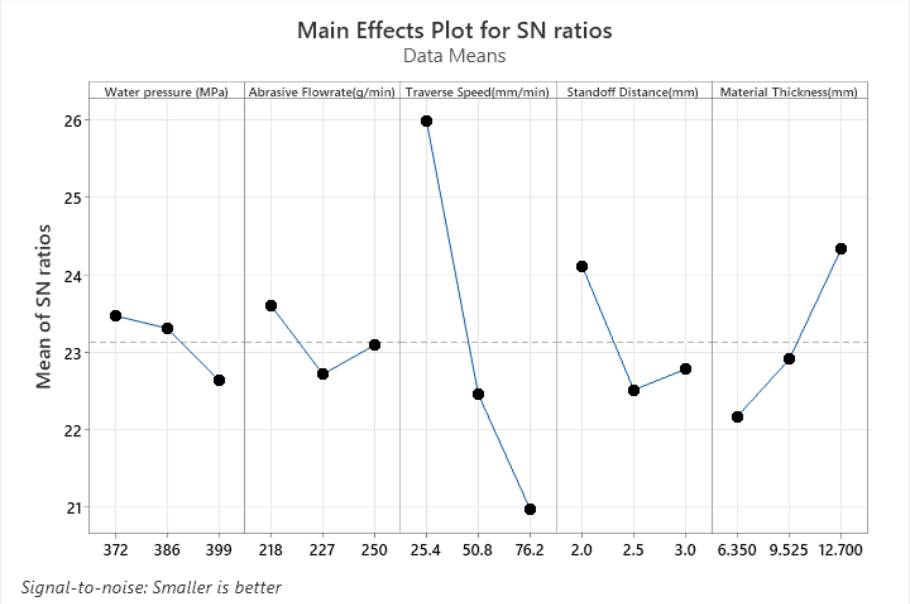

Figure 21. *Main Effect Plot for S/N Ratios – Kerf Angle*

Traverse speed stands out as the most influential factor, with a highly significant p-value of 0.000 and contributing 63.06% to the variability in the kerf angle. Material thickness also plays an important role, with a p-value of 0.003 and contributing 14.32% to the variability. Adjusting material thickness within the appropriate range can effectively control the kerf angle by reducing the angular deviation. Although standoff distance is less significant compared to traverse speed and material thickness, it demonstrates a considerable p-value ($p = 0.032$) and contributes 7.00% to the variability in the kerf angle.

Table 17. *Analysis of Variance for Kerf Angle*

Source	DF	Seq SS	Contribution	Adj SS	Adj MS	F-Value	P-Value
Water pressure (MPa)	2	0.000204	1.90%	0.000204	0.000102	1.17	0.335
Abrasive Flowrate(g/min)	2	0.000078	0.73%	0.000078	0.000039	0.45	0.647
Traverse Speed(mm/min)	2	0.006755	63.06%	0.006755	0.003377	38.83	**0.000**
Standoff Distance(mm)	2	0.000750	7.00%	0.000750	0.000375	4.31	**0.032**
Material Thickness(mm)	2	0.001534	14.32%	0.001534	0.000767	8.82	**0.003**
Error	16	0.001392	12.99%	0.001392	0.000087		
Total	26	0.010712	100.00%				

Note. Confidence level of 95%

The graph in Figure 22 illustrates the actual and predicted values for the taper angle. It visually compares the observed taper angles with those predicted by the model across different levels of the five and three factors. The actual values consistently appear to have large taper angles compared to the two predicted models. Building upon the earlier examination involving aluminum, which exhibited notable taper angles attributed to thickness, the carbon steel thickness investigated in this study spans from 6.350 to 12.700 mm. In comparison, aluminum ranges from 1.016 to 4.826 mm. It becomes apparent from the graph below that the kerf angle in this study displays sensitivity to thicker metals, which is particularly evident when compared to the predicted plot for aluminum.

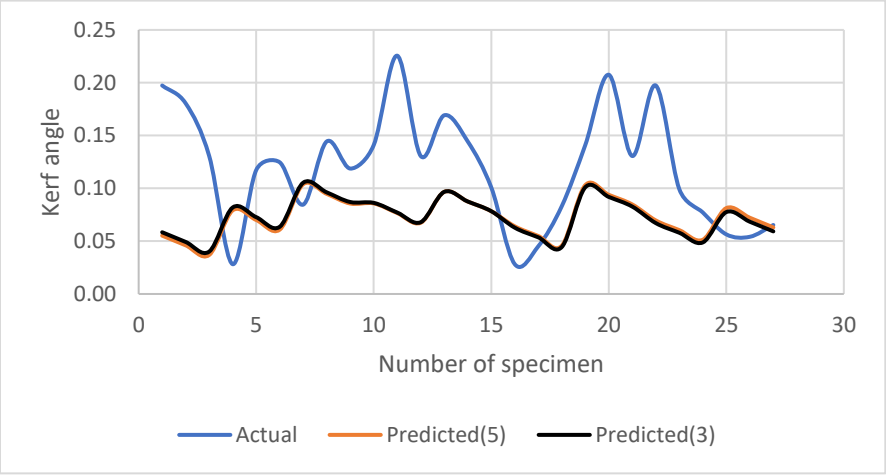

Figure 22. *Actual vs. Predicted data for 5 and 3 Factors Respectively*

4.3.3 Material Removal Rate (MRR)

Traverse Speed has the most substantial impact on MRR compared to the other factors considered in the study, with a delta value of 8.57. The significant influence of traverse speed variations on MRR highlights its critical importance as a factor to consider for optimization. Material thickness is another significant factor in the response, and it works closely with traverse speed to maximize the material removal rate.

Table 18. *Response Table for S/N Ratios - MRR*

Level	Water pressure (MPa)	Abrasive Flowrate(g/min)	Traverse Speed(mm/min)	Standoff Distance(mm)	Material Thickness(mm)
1	28.38	28.43	23.79	28.31	25.48
2	**28.57**	28.48	29.31	28.55	28.85
3	28.51	**28.55**	**32.36**	**28.60**	**31.12**
Delta	0.20	0.12	8.57	0.28	5.64
Rank	4	5	1	3	2

Note. Larger is better (S/N ratios)

The plot shows that the first and second factors, namely Traverse Speed and Material Thickness, significantly influence the S/N ratio. The steepness of the slope for certain factors in the main effect plot indicates their significant impact. Conversely, other factors such as Water Pressure, Abrasive flow rate, and Standoff Distance show slopes closer to the mean, suggesting their lesser influence on MRR than Traverse Speed and Material Thickness. The combination of factors Wp2-Af3-Ts3-Sd3-Mt3 represents the optimal configuration for maximizing MRR.

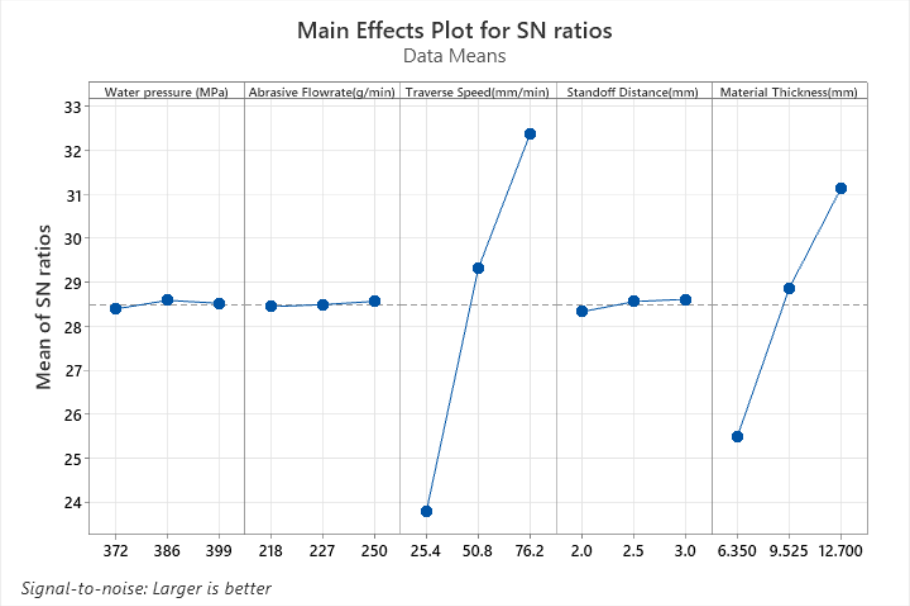

Figure 23. *Main Effect Plot for S/N Ratios - MRR*

Traverse speed and material thickness emerge as the most influential factors, with traverse speed contributing significantly (65.54%) to the variance and material thickness demonstrating substantial importance (30.66%). Conversely, water pressure and abrasive flow rate exhibit negligible contributions (0.01% and 0.00%, respectively), indicating their lack of significance. Standoff distance also shows minimal impact (0.04%) on the response.

Table 19. *Analysis of Variance for MRR*

Source	DF	Seq SS	Contribution	Adj SS	Adj MS	F-Value	P-Value
Water pressure (MPa)	2	0.55	0.01%	0.55	0.28	0.02	0.976
Abrasive Flowrate(g/min)	2	0.22	0.00%	0.22	0.11	0.01	0.990
Traverse Speed(mm/min)	2	3227.64	65.54%	3227.64	1613.82	140.38	**0.000**
Standoff Distance(mm)	2	2.11	0.04%	2.11	1.05	0.09	0.913
Material Thickness(mm)	2	1509.93	30.66%	1509.93	754.96	65.67	**0.000**
Error	16	183.94	3.74%	183.94	11.50		
Total	26	4924.39	100.00%				

Note. Confidence level of 95%

The predicted model, incorporating only two input factors (traverse speed and material thickness), exhibits an upward trend in Figure 24, with the highest Material Removal Rate

(MRR) observed. Following this, the model incorporating all factors displays a slightly lower MRR, while the experimental values consistently fall below this trend. The selected level settings for traverse speed likely resulted in an inconsistent representation of its influence on the MRR.

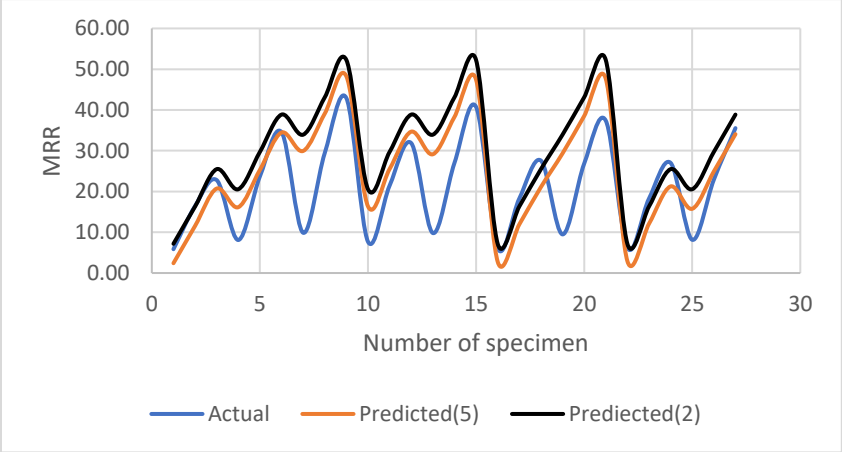

Figure 24. *Actual vs. Predicted data for 5 and 3 Factors Respectively*

4.3.4 Evaluation of Experimental Data

The probability plot in Figure 25 revealed a normal data distribution across all responses with p-values exceeding 0.05, indicating normality; further analysis can be conducted confidently.

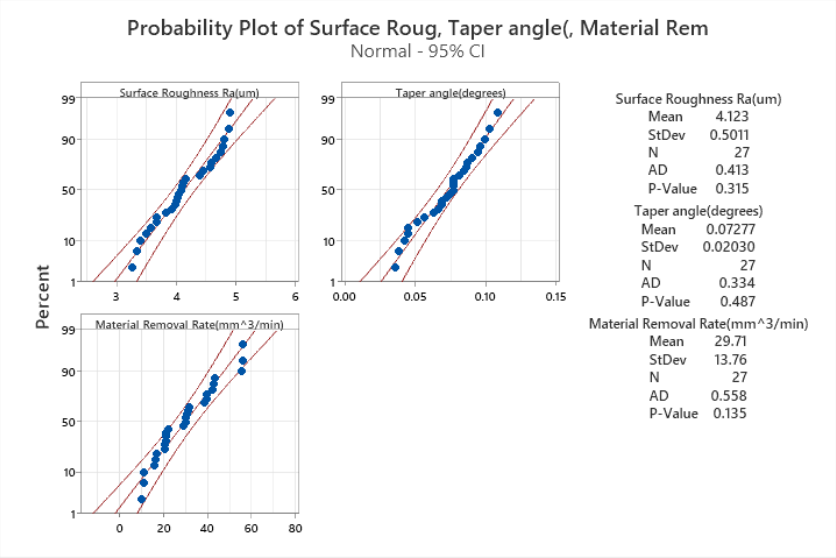

Figure 25. *Probability Plot for the Three Output Responses – 1020 Carbon Steel*

4.4 Summary of the Single Response Optimization for Both Metals

The analysis and subsequent validation experiments determined the optimal settings for each response variable, as depicted in Table 22. Notably, these optimal settings led to significant improvements in each response.

Table 20. *Results from the Optimal Settings for Each Response- Single Response Optimization*

Output response	Optimal Settings (Aluminum 6061-T6)	Result	Optimal settings (1020 Carbon Steel)	Result
Ra(μm)	P1A3T1S2M1 (344,127,76.20,2.50,1.016)	3.11	P2A3T2S1M1 (386,250,50.80,2,6.350)	3.20
Taper angle (˚)	P2A3T2S2M1 (361,127,101.6,2.50,1.016)	0.03	P1A1T1S1M3 (372,218,25.40,2,12.70)	0.05
MRR (mm^3/min)	P1A3T3D3M3 (344,127,127,3,4.826)	30.38	P2A3T3D3M3 (386,250,76.20,3,12.7)	40.77

For surface roughness (Ra), the optimal settings resulted in values of 3.11 μm for Aluminum 6061-T6 and 3.20 μm for 1020 Carbon Steel. Regarding taper angle, minimal angles of 0.03° and 0.05° were achieved for Aluminum 6061-T6 and 1020 Carbon Steel, respectively, with the optimal settings. Lastly, for Material Removal Rate (MRR), the optimal settings yielded values of 30.38 mm^3/min for Aluminum 6061-T6 and 40.77 mm^3/min for 1020 Carbon steel.

4.5 Taguchi- Grey Relational Analysis Optimization- Multi Response

Using Taguchi-Grey Relational Analysis for multi-responses such as MRR, kerf angle, and surface roughness provided a comprehensive understanding of how different input factors collectively impact various aspects of the machining process. Unlike single-response optimization, which focuses on optimizing one output at a time, multi-response optimization allows for a holistic approach. This approach considers the trade-offs between different responses and aims to find a balance that maximizes overall performance or quality. Simultaneously optimizing multiple responses guarantees that the selected settings yield an

optimal outcome across all pertinent factors, enhancing the robustness and efficiency of the machining process.

4.5.1 Aluminum 6061-T6

The highest Grey Relational Grade (GRG) was 0.825, ranked 1st among all the 27 experiments. Further optimization was carried out using the GRG as the new response, and the result was obtained, as shown in Table 23. Based on the analysis of the GRG optimization, the material thickness emerges as the most influential factor, as evidenced by its highest rank (1) and the most significant delta value (3.163). Various material thicknesses demonstrate the most critical impact on surface quality across the three output responses.

Table 21. *Response Table for S/N Ratios - GRG*

Level	Water pressure (MPa)	Abrasive Flowrate(g/min)	Traverse Speed(mm/min)	Standoff Distance(mm)	Material Thickness(mm)
1	-4.929	**-3.701**	-5.469	-4.813	-6.512
2	**-4.687**	-4.946	-4.807	-5.492	-4.539
3	-4.785	-5.754	**-4.125**	**-4.096**	**-3.350**
Delta	0.242	2.053	1.343	1.396	3.163
Rank	5	2	4	3	1

Note. Larger is better (S/N ratios)

The optimal setting for the five input factors that simultaneously optimize the three responses is denoted by Wp2-Af1-Ts3-Sd3-Mt3. This setting corresponds to water pressure at level 2 (361 MPa), abrasive flowrate at level 1 (45 g/min), traverse speed at level 3 (127 mm/min), standoff distance at level 3 (3 mm), and material thickness at level 3 (4.826 mm). These specific levels are chosen based on their collective ability to maximize the performance of all three responses, ensuring an efficient and effective machining process.

Figure 21 indicates the main effect plots for the signal-to-noise ratio of the GRA optimization for Aluminum 6061-T6

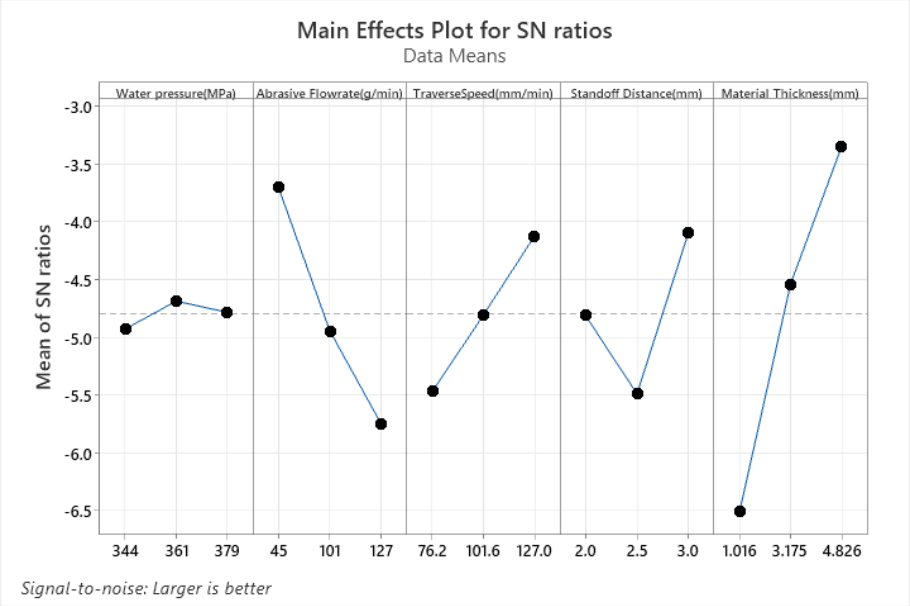

Figure 21. *Main Effect Plot for GRA Optimization*

Table 24 of ANOVA reveals several relevant factors with their respective p-values and contributions to the variation in output responses for aluminum machining. Among these factors, abrasive flow rate, traverse speed, standoff distance, and material thickness significantly influence the machining process. The abrasive flow rate demonstrates a notable contribution of 18.16% with a p-value of 0.004, followed by traverse speed with a contribution of 9.05% and a p-value of 0.043. Standoff distance also exhibits significance with a contribution of 7.97% and a p-value of 0.058. However, material thickness emerges as the most influential factor, boasting the highest contribution of 45.44% and a p-value of 0.000.

Table 22. *Analysis of Variance for GRA - Aluminum 6061-T6*

Source	DF	Seq SS	Contribution	Adj SS	Adj MS	F-Value	P-Value
Water pressure (MPa)	2	0.002861	0.69%	0.002861	0.001431	0.30	0.748
Abrasive Flowrate(g/min)	2	0.075297	18.16%	0.075297	0.037648	7.77	**0.004**
Traverse Speed(mm/min)	2	0.037515	9.05%	0.037515	0.018757	3.87	**0.043**
Standoff Distance(mm)	2	0.033063	7.97%	0.033063	0.016531	3.41	0.058
Material Thickness(mm)	2	0.188424	45.44%	0.188424	0.094212	19.45	**0.000**
Error	16	0.077514	18.69%	0.077514	0.004845		
Total	26	0.414674	100.00%				

Note. Confidence level of 95%

The regression model was generated with a fit regression model to quantify further the relationships between the input factors and the responses. The equation indicates that the GRA optimization for aluminum machining is influenced by abrasive flow rate (A_f), traverse speed (T_s), and material thickness (M_t). The coefficients associated with these factors provide insight into the magnitude of their effects on the surface quality.

Regression model

$$GRA\_O_{Al} = 0.3886 - 0.001543\ x\ A_f + 0.001774\ x\ T_s + 0.05352\ x\ M_t$$

4.5.2 1020 Carbon steel

The abrasive flow rate had the most significant impact on the quality of the machining process for 1020 carbon steel. Due to carbon steel's robust and durable nature, the increased abrasive particles in the pressurized water will affect its machining process.

Table 23. *Response Table for S/N Ratios - GRA*

Level	Water pressure (MPa)	Abrasive Flowrate(g/min)	Traverse Speed(mm/min)	Standoff Distance(mm)	Material Thickness(mm)
1	**-4.739**	-5.776	-5.010	**-4.525**	**-4.572**
2	-5.325	-5.020	**-4.429**	-5.522	-5.697
3	-4.958	**-4.225**	-5.583	-4.975	-4.753
Delta	0.586	1.551	1.153	0.998	1.125
Rank	5	1	2	4	3

Note. Larger the better (S/N ratio)

Based on the main effect plot depicted in Figure 24, the optimal input factors for achieving better responses in terms of Ra, kerf angle, and material removal rate were determined to be Wp1-Af3-Ts2-Sd1-Mt1: Water pressure at level 1(372 MPa), Abrasive flowrate at level 3 (250 g/min), Traverse speed at level 2 (60.80 mm/min), Standoff distance at level 1 (2 mm), and Material thickness at level 1 (6.350 mm).

Figure 26 indicates the main effect plot for the signal-to-noise ratio for the GRA optimization for 1020 carbon steel.

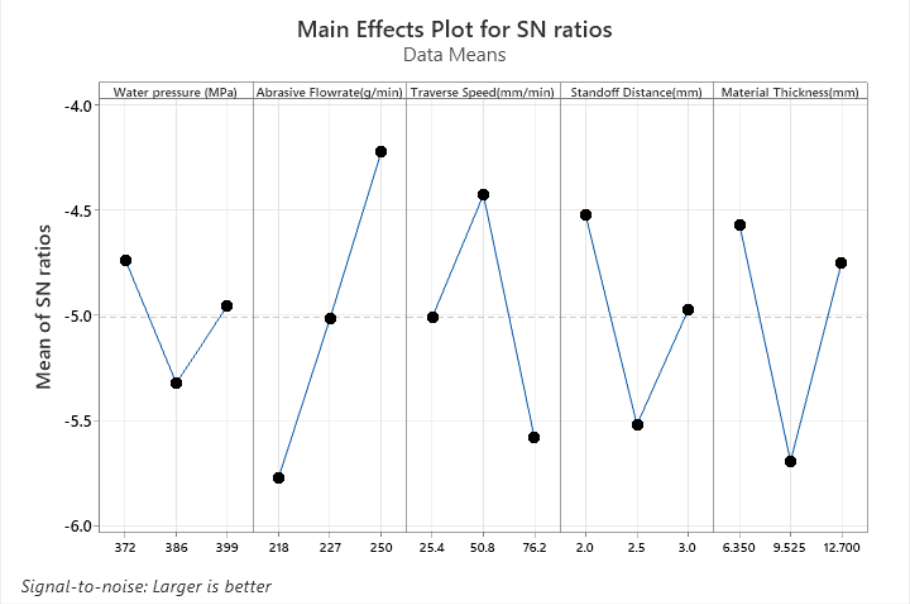

Figure 26. *Main Effect Plot for the GRA Optimization*

Abrasive flow rate, traverse speed, and Material Thickness were the most influential factors, as evidenced by their relatively low p-values (<0.05) and substantial contributions to the variation in GRA. In particular, the Abrasive flow rate contributes the largest variation at 25.79%, succeeded by Material Thickness at 15.23% and Traverse Speed at 14.14%. These findings suggest that adjusting these factors can significantly improve the machining process's

overall quality (Ra, Kerf angle, and MRR). However, Water Pressure and Standoff Distance exhibit higher p-values (>0.05), indicating weaker effects on the GRA.

Table 24. *Analysis of Variance for GRA- 1020 Carbon Steel.*

Source	DF	Seq SS	Contribution	Adj SS	Adj MS	F-Value	P-Value
Water pressure (MPa)	2	0.008071	4.85%	0.008071	0.004035	1.29	0.301
Abrasive Flowrate(g/min)	2	0.042946	25.79%	0.042946	0.021473	6.89	**0.007**
Traverse Speed(mm/min)	2	0.023545	14.14%	0.023545	0.011772	3.78	**0.045**
Standoff Distance(mm)	2	0.016740	10.05%	0.016740	0.008370	2.69	0.099
Material Thickness(mm)	2	0.025367	15.23%	0.025367	0.012683	4.07	**0.037**
Error	16	0.049877	29.95%	0.049877	0.003117		
Total	26	0.166546	100.00%				

Note. Confidence level of 95%

Since water pressure and standoff distance were not statistically significant, they were excluded from the regression model.

Regression model

$$GRO_{CS} = -0.064 + 0.00292\ x\ A_f - 0.000568\ x\ T_s - 0.00178\ x\ M_t$$

4.6 Summary for Both Optimization Methods

Table 27 compares single-response and multi-response optimization (MRO) outcomes using Taguchi-Grey Relational Analysis for Aluminum 6061-T6 and 1020 Carbon Steel. In the case of Aluminum 6061-T6, the multi-response optimization demonstrated slight improvements across all output responses (Ra, taper angle, and MRR) compared to single-response optimization. For 1020 Carbon Steel, the single response optimization yielded Ra, taper angle, and MRR values of 3.20 μm, 0.05 degrees, and 40.77 mm^3/min, respectively. After multi-response optimization, these metrics improved to 3.15 μm for Ra, 0.05 degrees for taper angle, and 42.26 mm^3/min for MRR.

Table 25. *Summary of Single Response and Multi Response Optimization (Taguchi-Grey Relational Analysis)*

Output responses	Aluminum 6061-T6	GRA MRO	1020 Carbon steel	GRA MRO
Ra(µm)	3.11	3.02	3.20	3.13
Taper angle (˚)	0.03	0.02	0.05	0.05
MRR (mm^3/min)	30.38	33.89	40.77	42.26

Note. GRA-MRO: Grey relational Analysis- Multi-response optimization

CHAPTER 5: DISCUSSION

The discussion section of this thesis focuses on the impact of material thickness on Abrasive Waterjet Machining (AWJM) output responses, namely surface roughness, kerf angle, and material removal rate. Through a thorough analysis of the results, the discussion supports the research objective by providing relevant insights into the relationship between material thickness and AWJM parameters. The following discussion draws upon relevant findings from previous research to examine the results and contribute to the existing knowledge base. The discussion section offers a comprehensive summary of the study's outcomes, highlighting key trends and observations that enhance our understanding of AWJM performance and material thickness variations.

5.1 Single Response Optimization

This optimization study aimed to analyze the effects of three key responses: surface roughness, kerf angle, and material removal rate relative to the five selected process factors: water pressure, abrasive flow rate, traverse speed, standoff distance, and material thickness. The investigation primarily focused on Aluminum 6061 and 1020 carbon steel. It became evident that these materials exhibited varying impacts on the surface quality of machined parts across their respective thickness levels.

5.2 Influence of material thickness on the output response

5.2.1 Surface Roughness (Ra)

Analyzing the signal-to-noise ratio and examining various factors for Aluminum 6061 T6 revealed a significant influence of material thickness on surface roughness. The obtained p-value for material thickness (0.002) was below the threshold of 0.05, indicating its substantial

contribution to the variation in Ra. Notably, a thickness of 1.016 mm for Aluminum was associated with comparatively lower surface quality than other thickness levels. This finding aligns with the study by *Khan and Gupta (2020)*, which suggests that achieving low surface roughness can pose challenges. Moreover, the results indicate a trend where surface roughness increases with thicker materials (*Edriys et al., 2020*).

On the other hand, material thickness tends to be an essential factor for obtaining low surface roughness for 1020 carbon steel; It was ranked as the main factor influencing Ra. Based on ANOVA, material thickness contributed about 84.78% to the variation since the thickness level ranges from 6.35 to 12.70 mm. However, the 6.35 mm machined parts achieved a low Ra metric, regarding this finding for the second metal. Conclusively, the relationship between material thickness and surface roughness reveals a direct proportionality. As the thickness of the material increases, there is a corresponding increase in surface roughness, indicating a deterioration in surface quality (*Pahuja et al., 2019*). Prior research has consistently demonstrated the impact of workpiece thickness on surface quality, aligning with the outcomes of this investigation conducted on aluminum 6061 T6 and 1020 carbon steel across three different thickness levels. Thinner metals consistently yielded desirable output responses in this study.

5.2.1 Kerf Angle

In the case of aluminum 6061 T6, material thickness emerges as the least influential factor regarding kerf angle, as indicated by the ANOVA results in Table 10. It does not exhibit statistical significance to the kerf angle. The primary significant factor affecting kerf angle is the abrasive flow rate. Previous research has consistently highlighted the importance of the type of abrasive particle in reducing kerf angle. An increase in the abrasive flow rate correlates with a

decrease in the kerf taper (Kumar & Kant, 2020). This study reveals that abrasive flow rate, particularly at level 3 (127 g/min), representing the maximum abrasive flow rate, is a prominent factor influencing kerf angle.

The analysis table identifies traverse speed as the primary influential factor affecting the kerf angle, followed by material thickness, as validated by the ANOVA results for 1020 carbon steel. Llanto et al. noted in their research that decreasing the traverse speed leads to a reduction in the kerf angle, although their study did not explore variations in thickness. This study reveals that level 1 (25.4 mm/min) from the response table's signal-to-noise ratio has the highest value, indicating that a slower movement of the cutting head over the workpiece results in a smaller kerf angle, consistent with findings by Vigneshwaran et al. (2018). Contrary to the study by Kusnurkar & Singh (2019), which suggested a reduction in kerf angle with thicker metal using different types of abrasive particles, our findings suggest that material thickness tends to correlate with a smaller kerf angle, particularly with thicker metals. Granite particles' cutting performance also closely resembles garnet material regarding kerf angles.

5.2.2 Material Removal Rate (MRR)

Material thickness accounts for a high variation in material removal rate, followed by traverse speed, which contributed 84.55% and 11.56% to MRR, respectively. The p-values for these factors are less than 0.05 (0.000), indicating statistical significance to the response for aluminum 6061-T6. The main effect plot for Signal-to-Noise (S/N) ratios in Figure () shows that thicker material and higher traverse speed maximize the volume of material removed per unit of time. This finding aligns with other studies by researchers. Edriys et al. concluded in their study that MRR had a direct correlation with thickness and the speed of the nozzle (traverse speed). According *to Fuset et al. (2021),* the MRR of 0.2304 g was achieved at a traverse speed setting

of 250 mm/min, corresponding to the highest-level settings. Compared to this study, the MRR was maximum at the highest traverse speed of 127 mm/min. Traverse speed significantly affects the Material Removal Rate (MRR) compared to other typical process input factors such as water pressure, abrasive flow rate, and standoff distance *(Shunmugasundaram et al., 2021*). Material thickness outperforms traverse speed in this study since material thickness was a relevant process input factor that was not included in most research works. A direct proportionality exists between the Material Removal Rate (MRR) and thickness.

In the analysis of 1020 carbon steel, similar factors influencing Material Removal Rate (MRR) were identified as in aluminum 6061 T6, with traverse speed and material thickness being significant. Traverse speed contributed 65.54% to MRR, holding the highest influence as the primary factor (Rank 1), while material thickness accounted for 30.66%. This inverse relationship compared to aluminum suggests differing machining characteristics between the materials. The traverse speed greatly influences the material removal rate, enabling faster machining and improved productivity, an essential factor in time-sensitive industries *(Gowthama et al., 2022*). Material thickness follows traverse speed in determining MRR, influencing the material removal volume. Optimizing traverse speed is essential for enhancing MRR and production efficiency in machining operations on 1020 carbon steel.

5.3 Multiple Response Optimization

The primary aim of this research is to explore the impact of material thickness on three key responses simultaneously: Ra, kerf angle, and MRR. Material thickness is the primary factor influencing the quality of the responses under study for aluminum 6061 T6. According to the response Table 23 for the Signal-to-Noise (S/N) ratio in optimizing the Grey Relational Grade, material thickness is an outstanding factor influencing all responses simultaneously. The ANOVA

Table 24 presents the significance of certain factors, namely material thickness, abrasive flow rate, and traverse speed, with p-values less than 0.05. Their contributions to the variation are 45.44%, 18.16%, and 9.05%, respectively. This suggests that these factors significantly impact the three output responses in single-response optimization scenarios. Another study indicates that higher Grey Relational Grade values are observed when the abrasive flow rate is at its highest level (*Gnanavelbabu et al., 2020*).

In the multi-response optimization for 1020 carbon steel, material thickness ranked third in importance based on the delta values from the response table. Abrasive flow rate emerged as the primary influencing factor, followed by traverse speed. These three process input factors are statistically significant to the responses, as evidenced by their p-values being less than 0.05 in the ANOVA Table 26. Similar factors were observed in the analyses for aluminum, although with differing contribution variations. Given the range of metal thickness studied for carbon steel, spanning from 6.35 to 12.7 mm, the quantity of abrasive particles mixed with water becomes a relevant consideration. This emphasizes setting the abrasive flow rate at its maximum level to achieve optimal results. Numerous researchers are actively developing industry optimization techniques using machine learning (*Deb et al., 2022*).

Due to various potential factors, water pressure might not have demonstrated significance in the study. One possible explanation could be the operating pressure range, which ranged from 344 to 399 MPa for both metals. However, the upper limit of this range aligns with the maximum operational capacity of the WARDJet machine. This limitation could have restricted the ability to detect any substantial effects on the outcomes, particularly considering the wide range of metal thicknesses studied, ranging from 1.016 to 12.70 mm.

5.4 Confirmation Test

After selecting the optimal level of the GRA optimization, another experiment was run using the optimal setting, and the result was compared to the single response optimization. The result for the three-response optimization using the single response is presented in Table 22, and that of the multi-response optimization in Table 27 with their respective settings. The comparison between single-response and multi-response optimization highlights the advantages of the GRA approach in achieving more comprehensive and balanced machining outcomes. While single-response optimization may be sufficient for addressing specific performance criteria individually, multi-response optimization offers a more integrated and efficient approach, leading to superior overall machining performance. These findings emphasize the importance of adopting advanced optimization methodologies, such as multi-response optimization, to enhance the machining process's efficiency and quality.

The limited number of experimental runs was a challenge in this study, as there were only 27 runs (Taguchi L27) for five process input factors with three levels each for both metals, with no replicates. This limited sample size made it difficult to adequately analyze the data and thoroughly explore the interactions between factors, particularly when considering the complexity of the process and the number of parameters being studied.

CHAPTER 6: Conclusion and Future Works

6.1 Conclusion of Study

The study draws key insights from Taguchi's Design of Experiment (DOE) and Grey Relational Analysis (GRA) optimization methodologies. While Taguchi DOE excels in optimizing individual responses, its limitation lies in achieving overall efficiency due to its focus on isolated factors and minimal attention to variable interactions. Conversely, GRA offers a more comprehensive approach by concurrently optimizing multiple responses, including surface roughness, kerf angle, and material removal rate (MRR). The research investigates the robustness of Grey Relational Analysis (GRA) in optimizing critical responses within the Abrasive Water Jet Machining (AWJM) process. GRA provides a systematic approach to improving multiple output responses simultaneously while considering the effects of various machining process parameters on aluminum and carbon steel, commonly used in industries.

6.2 Key Conclusions from the Study

1. The study highlights the significant influence of material thickness on output variables such as surface roughness, kerf angle, and material removal rate. Optimal machining parameters with specific thickness ranges were identified for aluminum and carbon steel. For aluminum (*1.016 to 4.826 mm*), optimal parameters included a water pressure of 361 MPa, abrasive flow rate of 45.0 g/min, traverse speed of 127.0 mm/min, and standoff distance of 3.0 mm. For carbon steel (*6.35 to 9.525 mm*), optimal parameters were a water pressure of 372 MPa, abrasive flow rate of 250 g/min, traverse speed of 50.8 mm/min, and standoff distance of 2.0 mm. These parameters were found to enhance surface quality significantly in machining operations.
2. The analysis indicated a direct relationship between MRR and material thickness, implying that as the material thickness increases, so does the MRR. Recognizing this

correlation is essential for streamlining machining processes to attain desired material removal rates efficiently.

3. The study found roughness commonly occurs in machined parts' exit region (Rough Cutting Region), especially noticeable in 1020 carbon steel due to energy dissipation. Using a maximum metal thickness of 12.70 mm and water pressures between 344 and 379, MPa highlighted the importance of Abrasive Water Jet Machining (AWJM) concerning high water pressures relative to the metal’s thickness and properties.
4. It was noted that roughness often occurs in the exit region (Rough Cutting Region) for 1020 carbon steel machine parts due to energy dissipation. The thickest metal used to study carbon steel was 12.70 mm within a water pressure of 344 and 379 MPa. Highlighting the importance of machining under high water pressure compared to metal thickness and its properties emphasizes the necessity of maintaining sufficient water jet pressure at the exit region of the material.
5. Some controlled variables, including water pressure, were determined to be insignificant within the specified level range. Despite their limited impact on the response variables at the designated input levels, it is essential to recognize their influence, especially in cases where roughness occurs at the exit region.
6. Measuring Ra is relatively straightforward but may only partially capture the actual surface roughness of AWJ machined parts with complex topography, as Rt does. While Ra focuses on the deviation over a specific sampling length, Rz (total roughness) considers the entire surface, providing a more comprehensive understanding of the roughness.

In future research stemming from this study, attention may be directed toward investigating the clamping style utilized for securing the workpiece during machining and conducting vibration analysis originating from the machining process. This exploration aims to deepen understanding of how different clamping methods influence machining outcomes and to identify potential sources of vibration-induced defects. Also, there is potential for exploring advanced optimization techniques, such as machine learning, to enhance the optimization process. Applying machine learning algorithms to analyze extensive datasets generated from full factorial experiments makes it possible to uncover intricate relationships between process parameters and output responses, thereby improving overall machining performance.

REFERENCES

Ahmed, T. M., El Mesalamy, A. S., Youssef, A., & El Midany, T. T. (2018). Improving surface roughness of abrasive waterjet cutting process by using statistical modeling. *CIRP Journal of Manufacturing Science and Technology*, *22*, 30–36. https://doi.org/10.1016/j.cirpj.2018.03.004

Arun, A., Rajkumar, K., Sasidharan, S., & Balasubramaniyan, C. (2023). Process parameters optimization in machining of monel 400 alloy using abrasive water jet machining. *Materials Today: Proceedings*, S2214785323045881. https://doi.org/10.1016/j.matpr.2023.08.308

Arun, M., Sathishkumar, N., Arunkumar, N., Jose, J. J., Fathah, I. A., & Kumar, K. N. (2021). Process parameters optimization in machining of duplex 2205 stainless steel alloy using AWJM technique. *Materials Today: Proceedings*, *46*, 1390–1395. https://doi.org/10.1016/j.matpr.2021.02.491

Bui, van H. (n.d.). *Strategies in 3 and 5-axis abrasive water jet machining of titanium alloys*.

Canbolat, A. S., Bademlioglu, A. H., Arslanoglu, N., & Kaynakli, O. (2019). Performance optimization of absorption refrigeration systems using Taguchi, ANOVA and Grey Relational Analysis methods. *Journal of Cleaner Production*, *229*, 874–885. https://doi.org/10.1016/j.jclepro.2019.05.020

Çetin, B. (n.d.). *PARAMETER SELECTION APPROACH AND OPTIMIZATION IN ABRASIVE WATER JET MACHINING*. 70.

Chakraborty, S., & Mitra, A. (2018). Parametric optimization of abrasive water-jet machining processes using grey wolf optimizer. *Materials & Manufacturing Processes*, *33*(13), 1471–1482. https://doi.org/10.1080/10426914.2018.1453158

Chandravadhana, S., Ohmsakthi Vel, R., Shameer, D., Kannappan, S., Nandhakumar, R., & Kalyanasundaram, R. (2021). Surface roughness prediction on drilled holes on strenx steel using AWJM process. *Materials Today: Proceedings*, *45*, 2419–2421. https://doi.org/10.1016/j.matpr.2020.10.838

Deb, J. (2024). *Data-Driven Prediction Modeling for Part Attributes and Process Monitoring in Additive Manufacturing*.

Deb, J., Ahsan, N., & Majumder, S. (2022). Modeling the Interplay Between Process Parameters and Part Attributes in Additive Manufacturing Process With Artificial Neural Network. *Volume 2A: Advanced Manufacturing*, V02AT02A015. https://doi.org/10.1115/IMECE2022-95120

Dekster, L., Karkalos, N. E., Karmiris-Obratański, P., & Markopoulos, A. P. (2023). Evaluation of the Machinability of Ti-6Al-4V Titanium Alloy by AWJM Using a Multipass Strategy. *Applied Sciences*, *13*(6), Article 6. https://doi.org/10.3390/app13063774

Edriys, I. I., Fattouh, M., & Masoud, R. (2020). Abrasive water jet machining of CFRPs: Single response optimization using taguchi method optimization. *IOP Conference Series. Materials Science and Engineering*, *973*(1). https://doi.org/10.1088/1757-899X/973/1/012029

Fuse, K., Chaudhari, R., Vora, J., Patel, V. K., & de Lacalle, L. N. L. (2021). Multi-Response Optimization of Abrasive Waterjet Machining of Ti6Al4V Using Integrated Approach of Utilized Heat Transfer Search Algorithm and RSM. *Materials*, *14*(24), Article 24. https://doi.org/10.3390/ma14247746

Gangadharan, G., Trivedi, D. S., & Vashi, O. (2022a). A Review on Optimization of Process Parameters in Abrasive Water Jet Machining/Cutting (AWJM) using various methods. *International Journal of Mechanical Engineering*, *7*.

Gangadharan, G., Trivedi, D. S., & Vashi, O. (2022b). A Review on Optimization of Process Parameters in Abrasive Water Jet Machining/Cutting (AWJM) using various methods. *International Journal of Mechanical Engineering*, *7*.

Girish, B. M., Siddesh, H. S., & Satish, B. M. (2019). Taguchi grey relational analysis for parametric optimization of severe plastic deformation process. *SN Applied Sciences*, *1*(8), 937. https://doi.org/10.1007/s42452-019-0982-6

Gnanavelbabu, A., Arunachalam, V., Surendran, K. T. S., & Saravanan, P. (2020). Optimization of Abrasive Water Jet Machining Parameters on AA6061/B4C/hBN Hybrid Composites using Grey-RSM. *IOP Conference Series: Materials Science and Engineering*, *764*(1), 012011. https://doi.org/10.1088/1757-899X/764/1/012011

Gómora, C. M., Ambriz, R. R., Curiel, F. F., & Jaramillo, D. (2017). Heat distribution in welds of a 6061-T6 aluminum alloy obtained by modified indirect electric arc. *Journal of Materials Processing Technology*, *243*, 433–441. https://doi.org/10.1016/j.jmatprotec.2017.01.003

Gowthama, K., Somashekar, H. M., Suresha, B., Rajole, S., & Ravindran, N. (2022). Optimization of abrasive water jet machining process parameters of Al 7071 using design of experiments. *Materials Today: Proceedings*, *52*, 2102–2108. https://doi.org/10.1016/j.matpr.2021.12.380

Hascalik, A., Çaydaş, U., & Gürün, H. (2007). Effect of traverse speed on abrasive waterjet machining of Ti–6Al–4V alloy. *Materials & Design*, *28*(6), 1953–1957. https://doi.org/10.1016/j.matdes.2006.04.020

Hidalgo, R., Esnaola, J., Larrañaga, M., Llavori, I., Herrero-Dorca, N., Hurtado, I., Otxoa, E., Rodríguez, P., & Kortabarria, A. (2018). *Influence of Surface Finish and Porosity on the Fatigue*

behaviour of A356 Aluminium Casting Alloy. *165*, 14007. https://doi.org/10.1051/matecconf/201816514007

Joel, C., & Jeyapoovan, T. (2021). Optimization of machinability parameters in abrasive water jet machining of AA7075 using Grey-Taguchi method. *Materials Today: Proceedings*, *37*, 737–741. https://doi.org/10.1016/j.matpr.2020.05.741

Joel, C., Joel, L., & Sankar, P. A. (2022). Investigation and Optimization of Process Parameters of Abrasive Water Jet Cutting on C360 Brass Alloy through Design of Experiments. *International Journal of Vehicle Structures & Systems*, *14*(3), 387–390. https://doi.org/10.4273/ijvss.14.3.21

Kant, R., & Dhami, S. S. (2021). Multi-Response Optimization of Parameters using GRA for Abrasive Water Jet Machining of EN31 Steel. *Materials Today: Proceedings*, *47*, 6141–6146. https://doi.org/10.1016/j.matpr.2021.05.053

Karkalos, N. E., Dekster, L., Kudelski, R., & Karmiris-Obratański, P. (2024). A Statistical and Optimization Study on the Influence of Different Abrasive Types on Kerf Quality and Productivity during Abrasive Waterjet (AWJ) Milling of Ti-4Al-6V. *Materials*, *17*(1), Article 1. https://doi.org/10.3390/ma17010011

Kehinde, A. J. (2021). Taguchi grey relational analysis on the mechanical properties of natural hydroxyapatite: Effect of sintering parameters. *The International Journal of Advanced Manufacturing Technology*, *117*(1–2), 49–57. https://doi.org/10.1007/s00170-021-07288-9

Khan, M. A., & Gupta, K. (2020). Machinability Studies on Abrasive Water Jet Machining of Low Alloy Steel for Different Thickness. *IOP Conference Series: Materials Science and Engineering*, *709*(4), 044099. https://doi.org/10.1088/1757-899X/709/4/044099

Kusnurkar, K. S., & Singh, J. S. S. S. (2019). Optimization of Input Parameters of AWJM: Using Three Different Abrasives on MS2062. *Non-Metallic Material Science*, *1*(1), Article 1. https://doi.org/10.30564/nmms.v1i1.892

Kuttan, A. A., Rajesh, R., & Anand, M. (2021). Abrasive water jet machining techniques and parameters: A state of the art, open issue challenges and research directions. *Journal of the Brazilian Society of Mechanical Sciences and Engineering*, *43*. https://doi.org/10.1007/s40430-021-02898-6

Llanto, J. M., Tolouei-Rad, M., Vafadar, A., & Aamir, M. (2021a). Impacts of Traverse Speed and Material Thickness on Abrasive Waterjet Contour Cutting of Austenitic Stainless Steel AISI 304L. *Applied Sciences*, *11*(11), Article 11. https://doi.org/10.3390/app11114925

Llanto, J. M., Tolouei-Rad, M., Vafadar, A., & Aamir, M. (2021b). Recent Progress Trend on Abrasive Waterjet Cutting of Metallic Materials: A Review. *Applied Sciences*, *11*(8), Article 8. https://doi.org/10.3390/app11083344

Manivannan, R., Department of Mechanical Engineering, Kalasalingam Academy of Research and Education, Krishnankoil, India., J, M., Department of Mechanical Engineering, Kalasalingam Academy of Research and Education, Krishnankoil, India., R, C., & Department of Physics, Kalasalingam Academy of Research and Education, Krishnankoil, India. (2019). Influence of AWJM Parameter on GFRP Reinforced Nylon-6 Composite. *International Journal of Engineering and Advanced Technology*, *9*(1s4), 903–906. https://doi.org/10.35940/ijeat.A1067.1291S419

Manoj, M., Jinu, G. R., & Muthuramalingam, T. (2018). Multi Response Optimization of AWJM Process Parameters on Machining TiB2 Particles Reinforced Al7075 Composite Using Taguchi-DEAR Methodology. *Silicon*, *10*(5), 2287–2293. https://doi.org/10.1007/s12633-018-9763-x

Nabavi, M. T., Moghaddam, M. A., Fardfarimani, N., & Kolahan, F. (2022). Comparative modeling of abrasive waterjet machining process based on OA-Taguchi and D-optimal approach and optimization using simulated annealing algorithm. *Scientia Iranica. Transaction B, Mechanical Engineering*, *29*(3), 1276–1287. https://doi.org/10.24200/sci.2021.58034.5529

Natarajan, Y., Murugesan, P. K., Mohan, M., & Liyakath Ali Khan, S. A. (2020). Abrasive Water Jet Machining process: A state of art of review. *Journal of Manufacturing Processes*, *49*, 271–322. https://doi.org/10.1016/j.jmapro.2019.11.030

Obinna Anayo, O., Salihi, A., Abdullahi, I., & Obada, D. (2022). Taguchi grey relational optimization of sol–gel derived hydroxyapatite from a novel mix of two natural biowastes for biomedical applications. *Scientific Reports*, *12*, 17968. https://doi.org/10.1038/s41598-022-22888-5

Ogbonna, O. S., Akinlabi, S. A., Madushele, N., Fatoba, O. S., & Akinlabi, E. T. (2023). Grey-based taguchi method for multi-weld quality optimization of gas metal arc dissimilar joining of mild steel and 316 stainless steel. *Results in Engineering*, *17*, 100963. https://doi.org/10.1016/j.rineng.2023.100963

Ozcan, Y., Tunc, L. T., Kopacka, J., Cetin, B., & Sulitka, M. (2021). Modelling and simulation of controlled depth abrasive water jet machining (AWJM) for roughing passes of free-form surfaces. *The International Journal of Advanced Manufacturing Technology*, *114*(11), 3581–3596. https://doi.org/10.1007/s00170-021-07131-1

Padhy, C., & Singh, P. (2020). Use of Multi-Objective Optimization Technique (Taguchi-GRA Approach) in Dry Hard Turning of Inconel 625. *INCAS BULLETIN*, *12*, 133–142. https://doi.org/10.13111/2066-8201.2020.12.2.11

Pahuja, R., Ramulu, M., & Hashish, M. (2019). Surface quality and kerf width prediction in abrasive water jet machining of metal-composite stacks. *Composites Part B: Engineering*, *175*, 107134. https://doi.org/10.1016/j.compositesb.2019.107134

Pal, H., Singh, H., & Kumar, J. (2017a). *Optimization of process parameters of abrasive water jet machining process for Dimension Deviation by Taguchi's parameter design approach*. 9.

Pal, H., Singh, H., & Kumar, J. (2017b). *Single Response optimization of abrasive waterjet machining process by Taguchi's parameter design approach*.

Patel G C, M., Jagadish, Rajana..Kgp, S., & Nv, S. N. (2020). *Optimization of Abrasive Water Jet Machining for Green Composites Using Multi-variant Hybrid Techniques* (pp. 129–162). https://doi.org/10.1007/978-3-030-19638-7_6

Pon Selvan, M. C., Sampath, S. S., Madara, S. R., & Raj, N. S. S. (2018). Effects of process parameters on depth of cut in Abrasive Waterjet Cutting of phosphate glass. *2018 Advances in Science and Engineering Technology International Conferences (ASET)*, 1–6. https://doi.org/10.1109/ICASET.2018.8376868

Qazi, M. I., Akhtar, R., Abas, M., Khalid, Q. S., Babar, A. R., & Pruncu, C. I. (2020). An Integrated Approach of GRA Coupled with Principal Component Analysis for Multi-Optimization of Shielded Metal Arc Welding (SMAW) Process. *Materials*, *13*(16), 3457. https://doi.org/10.3390/ma13163457

Radovanović, M. (2020). Multi-Objective Optimization of Abrasive Water Jet Cutting Using MOGA. *Procedia Manufacturing*, *47*, 781–787. https://doi.org/10.1016/j.promfg.2020.04.241

Ravi Kumar, K., Sreebalaji, V. S., & Pridhar, T. (2018). Characterization and optimization of Abrasive Water Jet Machining parameters of aluminium/tungsten carbide composites. *Measurement*, *117*, 57–66. https://doi.org/10.1016/j.measurement.2017.11.059

S. Alsoufi, M. (2017). State-of-the-Art in Abrasive Water Jet Cutting Technology and the Promise for Micro- and Nano-Machining. *International Journal of Mechanical Engineering and Applications*, *5*(1), 1. https://doi.org/10.11648/j.ijmea.20170501.11

Saravanan, S., Vijayan, V., Suthahar, S. T. J., Balan, A. V., Sankar, S., & Ravichandran, M. (2020). A review on recent progresses in machining methods based on abrasive water jet machining. *Materials Today: Proceedings*, *21*, 116–122. https://doi.org/10.1016/j.matpr.2019.05.373

Senthil Kumar, R., Gajendran, S., & Kesavan, R. (2020). Evaluation of Optimum Machining Parameters by AWJM for Granite through Multi Response Methods. *Materials Today: Proceedings*, *22*, 3056–3066. https://doi.org/10.1016/j.matpr.2020.03.441

Senthilkumar, T. S., Muralikannan, R., & Senthil Kumar, S. (2020). Surface morphology and parametric optimization of AWJM parameters using GRA on aluminum HMMC. *Materials Today: Proceedings*, *22*, 410–415. https://doi.org/10.1016/j.matpr.2019.07.404

Shastri, A., Nargundkar, A., & Kulkarni, A. (2021). *Optimization of Abrasive Water Jet Machining (AWJM)* (pp. 77–86). https://doi.org/10.1007/978-981-15-7797-0_5

Shukla, R., & Singh, D. (2017). Experimentation investigation of abrasive water jet machining parameters using Taguchi and Evolutionary optimization techniques. *Swarm and Evolutionary Computation*, *32*, 167–183. https://doi.org/10.1016/j.swevo.2016.07.002

Silva, P. S. da, Senna, L. F. de, Gonçalves, M. M. M., & Lago, D. C. B. do. (2019). Microbiologically-Influenced Corrosion of 1020 Carbon Steel in Artificial Seawater Using Garlic Oil as Natural Biocide. *Materials Research*, *22*, e20180401. https://doi.org/10.1590/1980-5373-MR-2018-0401

Spadło, S., Bańkowski, D., Młynarczyk, P., & Hlaváčová, I. M. (2021). Influence of Local Temperature Changes on the Material Microstructure in Abrasive Water Jet Machining (AWJM). *Materials*, *14*(18), Article 18. https://doi.org/10.3390/ma14185399

Tisza, M., & Czinege, I. (2018). Comparative study of the application of steels and aluminium in lightweight production of automotive parts. *International Journal of Lightweight Materials and Manufacture*, *1*(4), 229–238. https://doi.org/10.1016/j.ijlmm.2018.09.001

Tiwari, T., Sourabh, S., Nag, A., Dixit, A. R., Mandal, A., Das, A. K., Mandal, N., & Srivastava, A. K. (2018). Parametric investigation on abrasive waterjet machining of alumina ceramic using response surface methodology. *IOP Conference Series. Materials Science and Engineering*, *377*(1). https://doi.org/10.1088/1757-899X/377/1/012005

Vigneshwaran, S., Uthayakumar, M., & Arumugaprabu, V. (2018). Abrasive water jet machining of fiber-reinforced composite materials. *Journal of Reinforced Plastics and Composites*, *37*(4), 230–237. https://doi.org/10.1177/0731684417740771

Viswanath, J., Tulasi, C. L., & Kumba, A. (2018). Optimizing the process parameters of AWJM using Taguchi method and ANOVA on Inconel 625. *ARPN Journal of Engineering and Applied Sciences*, *13*, 1578–1586.

Xiaochu, L., Zhongwei, L., Guilin, W., & Xuefeng, Y. (2019). Waterjet machining and research developments: A review. *The International Journal of Advanced Manufacturing Technology*, *102*(5–8), 1257–1335. https://doi.org/10.1007/s00170-018-3094-3

µMachining, µMachining. (n.d.). What is Stand-Off Distance (SOD)? Explain Its Effect on AJM Performance. *Minaprem.Com*. Retrieved April 8, 2024, from https://www.minaprem.com/micro-machining/ajm/what-is-stand-off-distance-sod-explain-its-effect-on-ajm-performance/